DESIGN AND EXPERIMENTAL EVALUATION

OF A HIGH ENERGY DENSITY ELASTOMERIC

STRAIN ENERGY ACCUMULATOR

By

John Michael Tucker

Thesis

Submitted to the Faculty of the

Graduate School of Vanderbilt University

in partial fulfillment of the requirements

for the degree of


MASTER OF SCIENCE

in

Mechanical Engineering

May, 2012

Nashville, Tennessee


Approved:

Professor Eric J. Barth

Professor Thomas J. Withrow

Professor Robert J. Webster

This thesis is dedicated to my Lord and God Jesus Christ, for whose glory it was

attempted and by whose grace it was completed.

# ACKNOWLEDGEMENTS

## TABLE OF CONTENTS

LIST OF FIGURES

# LIST OF TABLES

CHAPTER 1

## Introduction

### 1. <u>Hydraulic Accumulators</u>

All energetic systems, whether they be mechanical, electric, hydraulic, or some combination can be expressed in terms of effort $e$ and flow $f$. The power transferred from one energetic element to the next is always a product of these two elements, force and velocity, voltage and current, pressure and volumetric flow rate. Since energy is the time integral of power, energy transfer can simply be measured as the integral of this product over time. The relationship between effort and flow is a reactionary one, governed by the properties of each system element. For potential energy storage elements, this relationship is an algebraic function between effort and the integral of flow, force and displacement for springs, voltage and charge for capacitors, pressure and volume change for hydraulic accumulators. Just as spring constants dictate the force-displacement relationship of springs, bulk modulus—the inverse of compressibility— dictates the relationship between pressure and volume change in hydraulic accumulators. Since hydraulic fluid itself has a very high bulk modulus, miniscule changes in the volume of a closed hydraulic system result in large swings in pressure. Pump-motor noise can cause unsafe pressure fluctuations in this way if unaccounted. Commercial hydraulic accumulators remedy this by providing temporary storage for this oscillating flow in a device with a much more favorable pressure-volume change relationship.

Because they contain bags of compressible gas, these accumulators have a much lower

effective bulk modulus and thus respond to small changes in volume with much smaller

changes in pressure.
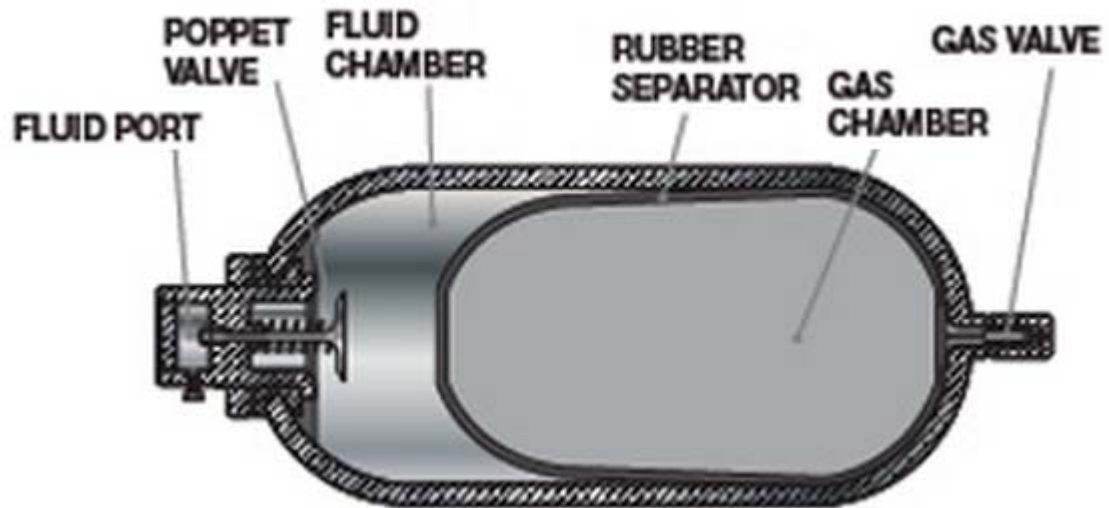


Figure 1 Hydraulic Gas Accumulator (Tobul)

Bond Graph theory tells us that for potential storage elements, the relation of

effort and flow can be written thus: (Karnopp 18)

$$e = \frac{1}{C} * \int f \tag{1}$$

Where $C$ is a capacitive factor, capacitance in the case of capacitors, compliance in the

case of springs, and compressibility in the case of pressure vessels (Karnopp 52).

Furthermore, when written in this form, the capacitive factors of multiple elements can be

easily combined analytically. When N elements meet at a junction of common effort, the

result is:

2

$$C_{effective} = \sum_{i=1}^{N} C_i \tag{2}$$

This can most easily observed in the case of capacitors arranged in a parallel circuit. Each capacitor stores the same amount of charge as it would if the other parallel branches were removed, because each capacitor sees the same effort (voltage) as the next. Therefore, the total capacitance of the circuit is equal to the sum of capacitance. Springs in parallel likewise share a common effort junction, the reaction forces between a series of springs in series are all the same tension force or compressive force. Thus their compliances add together to yield an effective compliance. When written in terms of stiffness, the inverse of compliance, this sum becomes the inverse of a sum of inverses, and the same is true for bulk modulus, the inverse of compressibility.

$$\frac{1}{C_{effective}} = \frac{1}{\sum_{i=1}^{N} \frac{1}{C_i}} \tag{3}$$

Accumulators share a common effort (pressure) junction with the main hydraulic lines, and so the effective compressibility of the system is therefore the sum of the component compressibilities, and the effective bulk modulus is the inverse of the sum of inverse bulk moduli. Since the compressibility of an accumulator is much higher than that of hydraulic fluid, the bulk modulus of the system is dramatically reduced. With a low effective bulk modulus, the pressure of the system remains relatively constant, despite slight fluctuations in volume.

## 2. Hydraulic Regenerative Braking

While the filtering out of high frequency pressure noise from a system is certainly an appropriate application of a hydraulic accumulator, these accumulators have recently received increased attention for their potential for steady state energy storage. Compressed nitrogen gas accumulators, which use hydraulic fluid to compress a gas-filled elastomeric bladder to pressures up to 5000 psi have been commercialized by Eaton Corp. for use in hydraulic hybrid refuse trucks. This method for regenerative braking called Hydraulic Launch Assist (HLA) uses reversible pump motors to pump fluid from a reservoir into a high pressure accumulator, which stores the pump energy in the compressed nitrogen. The kinetic energy of the trucks is in this way converted into stored potential energy as the pumps slow the vehicle down. When the accelerator is pressed, the pump direction is reversed and the high pressure fluid stored in the accumulator returns to the reservoir. On the way back, this pressure and flow drives the pumps (now acting as motors), accelerating the vehicle back up to speed. This accumulator design has been demonstrated to "reduce fuel consumption by up to 1500 gallons per truck annually, depending on duty cycle (Eaton)."

While these accumulators have been demonstrated as a cost effective method of regenerative braking in refuse trucks, they do not scale properly for use in small passenger vehicles. When empty, refuse trucks can weigh in at more than 25000 lbs, but their average driving speed may lie between 10 and 15 mph. Compare this to a small passenger vehicle which weighs on the order of 3500 lbs and drives at an average speed on the order of 35 mph (a conservative estimate based on urban driving). The kinetic

energy of the refuse truck in this case would average somewhere between 120 and 250 kJ, while the passenger vehicle, though 86% lighter, would average at right around 200 kJ. Because the energy storage requirements are nearly identical, the HLA system cannot be scaled down in its current form. Its weight alone, 1650 lbs all told, would increase the weight of a sedan by more than 50%. The search for improving accumulator technology is ongoing. (Toulson 2008)

One possible solution to system scaling, however, lies in switching energy storage domains entirely. Just as electrical hybrids store their energy in electric charge and chemical batteries, and Eaton accumulators store their energy in thermal energy of compressed gas, this thesis explores the domain of mechanical energy storage, that is to say the strain energy of deformed materials. There are multiple potential advantages of material strain as an energy storage method. By staying within the domain of mechanical energy, much of the losses and complications associated with energy domain conversions—from mechanical to electric to chemical and back for example—are removed. Crucially, the strain-energy domain also has the potential for much higher energy densities, as will be shown. Lastly, the strain-energy domain gives opportunity for modifying effort-flow profiles pre-transmission. This last advantage will be discussed at length in chapter 5.

### 3. <u>Strain Energy Density</u>

In the design of a hydraulic energy accumulator for regenerative braking energy storage, three properties are paramount, energy density (both volumetric and gravimetric)

and efficiency. High volumetric energy density is required in order for the device to fit on a compact car. High gravimetric energy density is equally important so that the device does not add too much weight to the car. High efficiency is of course essential, since energy return is the only benefit gained over traditional dissipative brakes. Efficient energy return translates into direct fuel savings especially in urban driving conditions. In the case of an elastomeric strain energy accumulator—where the material being strained is a high performance elastic polymer—volumetric and gravimetric energy densities can be considered to be roughly equivalent, since the density of both the working fluid and the elastomer are near enough to 1000 Kg/m$^3$. The energy density of the accumulator as a whole is defined to be the total energy storage capacity of the device divided by the volume of the system.

$$e_{System} = \frac{E_{Stored}}{\forall_{System}} \tag{4}$$

It is convenient to define a metric whereby individual elastomeric materials can be compared solely based on their stress-strain properties apart from the rest of the accumulator. To this end the energy density of a material is here defined to mean the energy storage capacity of the material per unit volume of the material. Since all of the elastomers in question are virtually incompressible (though quite deformable), volume can be treated as a constant. In order to pin down material energy density in terms of stress and strain, consider the case of a constant cross-section specimen with one end fixed and the other end being pulled in tension by a force $F$. A material stressed in tension deforms from an initial area $A_0$ and length $l_0$ to a new area $A$ and length $l$. The

6

stress required to create this deformation $\sigma$ is defined to be the force divided by the initial area. The strain $\varepsilon$ is defined to be the change in length divided by the initial length. Since energy is the integral of force over a distance, the differential change in strain energy can be written as

$$dE = F * dl = (\sigma * A_0) * (d\varepsilon * l_0) = \forall_0 * \sigma * d\varepsilon \tag{5}$$

Where $\forall_0$ is the constant volume of the elastomer. Integrating both sides and dividing by $\forall_0$ yields

$$\frac{E}{\forall_0} = \int_0^\varepsilon (\sigma) d\varepsilon \tag{6}$$

This term on the left is the very definition of material energy density of a material $e_M$ which is in the general case equal to the integral under a stress-strain curve from one strain state to another.

$$e_M = \frac{E_{Stored}}{\forall_M} = \int_{\varepsilon 1}^{\varepsilon 2} (\sigma) d\varepsilon \tag{7}$$

This definition is equivalent to the definition of material toughness for metals which defines the amount of energy a metal can absorb by plastically deforming before failure. The difference here is that in the case of strain-energy density, an elastomer must be able to return itself from $\varepsilon 2$ to $\varepsilon 1$ elastically without weakening and thus $\varepsilon 2$ is significantly lower than the maximum elongation before break.

Hydraulic energy transfer is defined as the integral of fluid pressure over a change in volume. Because of this, the required volume of the working fluid $\forall_F$, in relation to the energy stored, can be expressed as an average pressure—with the same units as energy density—by reducing the equation for fluid power transfer by way of the mean value theorem.

$$\frac{E_{Stored}}{\forall_F} = \frac{1}{\forall_F}\int_0^{\forall_F}(P)d\forall_F = \frac{\forall_F}{\forall_F}P_{average} = P_{average} \tag{8}$$

Thus the total volume of the system can be expressed as a sum involving the energy storage capacity, the elastomeric energy density, the average fluid pressure, and whatever extra volume, called dead volume, which contributes neither to the energy transfer nor energy storage. This dead volume $\forall_D$ includes such things as the pressure vessels, hydraulic fittings, valves, and other miscellaneous components common to all hydraulic accumulators as well as any elastomeric material that does not store and release energy.

$$\forall_{System} = \forall_M + \forall_F + \forall_D = \frac{E_{Stored}}{e_M} + \frac{E_{Stored}}{P_{average}} + \forall_D \tag{9}$$

The total system energy density, therefore, is a function which increases with increasing average pressure and elastomeric energy density and decreases with increasing dead volume.

8

$$e_{System} = \frac{E_{Stored}}{\frac{E_{Stored}}{e_M} + \frac{E_{Stored}}{P_{average}} + \forall_D} = \frac{1}{\frac{1}{e_M} + \frac{1}{P_{average}} + \frac{\forall_D}{E_{Stored}}} \tag{10}$$

If desired, additional figures of merit can be obtained by incorporating efficiency into equations for material and system energy density. For example, by defining $e_{Returned}$ as the energy a material specimen is capable of returning per unit volume of material, the equation for $e_{Returned}$ can be derived from equation (7):

$$e_{Returned} = \frac{E_{Returned}}{\forall_M} = \int_{\varepsilon 2}^{\varepsilon 1} (\sigma) d\varepsilon \tag{11}$$

Note that because strain of materials is not a perfectly efficient process, $e_{Returned} < e_M$.

## 4. Prior Work

The work reported in this thesis is a continuation of prior research done by Alexander Pedchenko. In his thesis he utilized Granta Material Intelligence CES material selection software to approximate the range of possible strain energy densities of materials, both gravimetric and volumetric. He observed that polyurethanes and natural rubbers were the top contenders in both categories and used polyurethanes and latex rubbers for his proof of concept prototypes. In addition to his research into material selection, he utilized finite element analysis techniques and small-scale prototypes to explore the efficiency of elastomeric accumulators and the unusual effort-flow relationship demonstrated by the inflation of an elastomeric bag. This simple bladder design, which will be discussed in more detail in chapter 5, was the original motivation

9

behind this research. In short, it behaves similarly to a constant-force spring, with effort remaining maximized throughout a large range of flow. While gas accumulators used as pressure filters keep pressure nearly constant throughout small oscillations in volume, their pressure-volume profile on a larger scale is closer to an exponential curve than a constant value (Figure 2), with pressure increasing at an increasing rate as volume is decreased. Elastomeric bladders, on the other hand, maintain a nearly constant pressure throughout inflation, a phenomenon which will also be discussed in greater detail in chapter 5. It is mentioned here in conjunction with equation (8) to present one of the motivating factors for the development of strain-energy accumulators, optimization of effort-flow profiles. Equation (8) shows the significance of maximizing average effort in the reduction of flow volume, and as Figure 2 demonstrates, strain-energy accumulator design opens the door to doing just that.
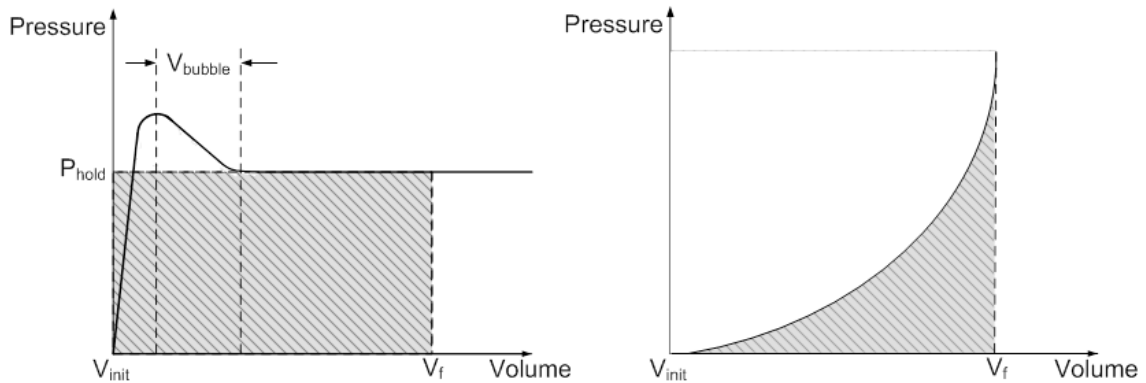


Figure 2 Ideal Strain-Energy Bladder Compared to Gas Accumulator

Two important technologies also came forth from this initial research. The first, called the "series accumulator configuration" is a method for scaling the pressure profile of a strain-energy accumulator by combining accumulator stages in series. The

surrounding environment of each stage, rather than atmospheric pressure, is the inlet fluid to the next stage. The strain in each stage, when charged, causes a pressure differential across the stage. Since hard elastomers are virtually incompressible under hydrostatic pressure, these differential pressures can add in series without straining each stage any more than the previous one. In this way, the inlet to a series of N accumulator stages would experience N times the effort of a stand-alone stage for the same flow. This theory was validated via prototype by linking two latex bladder prototype stages together in series and comparing the pressure-volume curve of the combined pair to that of a single stage. (Pedchenko 3.2.5)
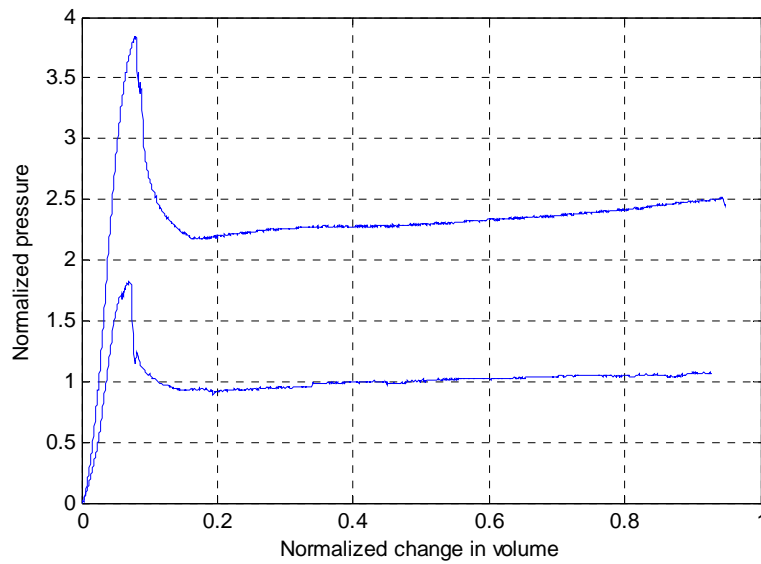


Figure 3 Series Configuration Pressure (Pedchenko 2011)

The second key innovation which gives strain-energy accumulators an edge over gas-bladder accumulators is the concept of an integrated reservoir. Gas-bladder accumulators require separate volumes for low pressure fluid and high pressure fluid. They must pump fluid from one reservoir into another of equal size in order to function.

11

In a strain-energy accumulator, the material being strained can form the barrier between high pressure fluid and low pressure fluid.  In this way, a single reservoir is often all that is required.  The fluid on one side of the material divider is pumped to the other side of the divider at a much higher pressure.  As the ratio of volumes across the divide shifts, the divider strains from one side of the reservoir to the other.  No net fluid ever leaves the reservoir; it merely relocates to the other side of a moving barrier.  This is easiest to see in the case of the simple bladder, anchored to one end of a cylindrical reservoir, inflated by a pump connected to the other end of the cylinder.  Though the bladder inflates and stretches to the very end of the reservoir, the total volume of the system never changes.
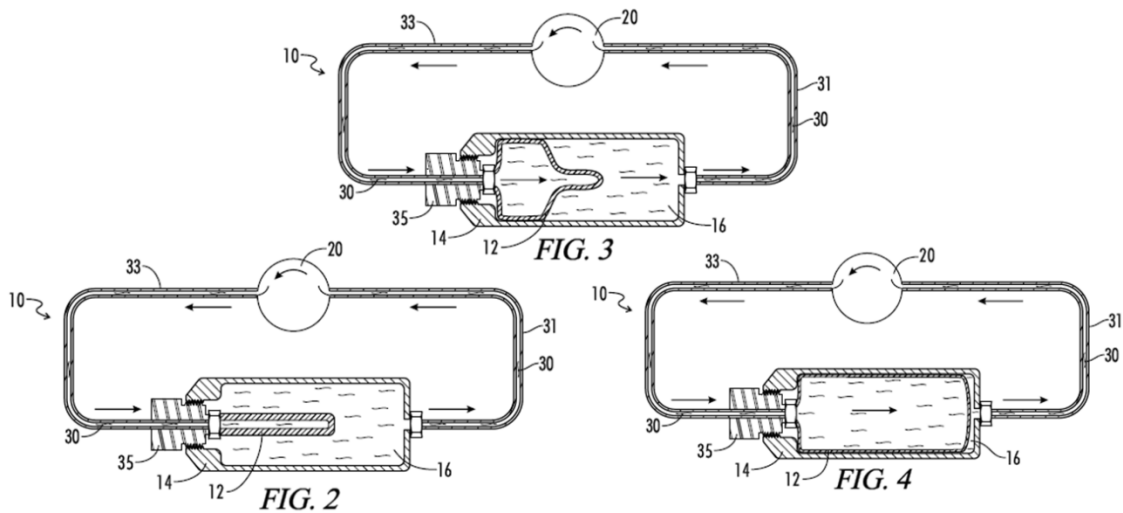


Figure 4 Integrated Reservoir Schematic (Pedchenko 2011)

CHAPTER 2


**Material Candidates**


1. <u>Polyurethane background</u>


Elastomers are polymers with very high yield strains, capable of reversible extension of over 600% in some cases. They owe this elasticity to their long polymer chains and covalent cross-links. When an elastomer is strained, the cross-links, which force neighboring chains to remain joined at various points, cause the chains to bend and stretch elastically rather than sliding and shifting permanently. When released, the elastomer returns to its original configuration. Some common elastomers include natural and synthetic rubber (polyisoprene), polybutadiene, nitrile rubber, silicone rubber, and polyurethane.

Thermoset polyurethanes in particular have excellent mechanical properties including high elasticity and abrasion resistance. They also have good chemical compatibility. Their high strength and elongation, combined with their efficient energy return make them prime candidates for development of an elastomeric strain energy accumulator. (Pleiger)

For comparison, consider an approximation of the strain energy density $e_M$, as defined above, in the case of polyurethane and also spring steel. $e_M$ for spring steel—it being a linearly elastic material—can be approximated by the area under a line with height equal to the yield strength and slope equal to the modulus of elasticity.

$$\varepsilon = \sigma_y/E \qquad (12)$$

Assuming $\sigma_y$ = 500 MPa and E = 210 GPa, $\varepsilon$ =0.24% and $e_M$ = 0.60 MPa. As will be shown below, $e_M$ for polyurethanes can exceed 15 MPa, twenty five times the strain energy density of spring steel. This does not even take into account the fact that polyurethane has less than one sixth the density of steel, whose gravimetric energy density is therefore lower still.

## 2.  Reported properties vs. cyclical properties

One significant hindrance to the selection of a particular elastomer is the frequent disparity between reported static properties of a tested material and the desired cyclical properties. For hyperelastic materials, ultimate tensile strength is not always an accurate indicator of relative fatigue strength, especially when the roll of strain rate cannot easily be quantified. Furthermore, the material softening that hyperelastic materials experience under cyclical loading, termed the Mullins effect, makes the quantification of strain energy density impossible to derive from tensile strength and elongation alone, because these properties give no indication as to the rest of the stress-strain profile. When an elastomer is loaded to a stress which it has not previously experienced—which is the case for all stresses during the first cycle of testing—it softens somewhat. While the material will deform to roughly the same strain at that particular stress, all of the stresses leading up to that point will have higher strain values than corresponding stresses of the first

14

cycle. This effect is neither proportional nor well understood, and as such the cyclical stress-strain profile of an elastomer cannot be extrapolated from a single extension test, much less the ultimate tensile strength and stress. In 2008 a review article was published in the European Polymer Journal which consisted of a comprehensive review of the Mullins effect from both experimental and also model based approaches. This excerpt summarizes the methodologies and conclusions surrounding and investigation of the Mullins effect in the case of a styrene-butadiene rubber (SBR). This synthetic elastomer shares much in common with polyurethane and serves as an instructive example of the Mullins effect: (Diani 2009)

In order to illustrate the material softening resulting from the Mullins effect, cyclic uniaxial tension tests were performed on a sulfur-vulcanized SBR filled with 50 phr of N220 carbon-black. Flat tensile samples were cut from SBR compression molded sheets. Uniaxial tension tests were performed on a GTest 810 tensile machine operated in a local strain control mode through VideoTraction image analysis. Tests were run at a low constant strain rate of $10_{-3}$ $s_{-1}$. One sample was submitted to a simple uniaxial tension test, while another one was submitted to a cyclic uniaxial tension test with the maximum stretching increasing every 5 cycles. Fig. 1 presents the stress‑strain responses of both samples. In Fig. 1, we observe a softening that is specific to materials exhibiting the Mullins effect:
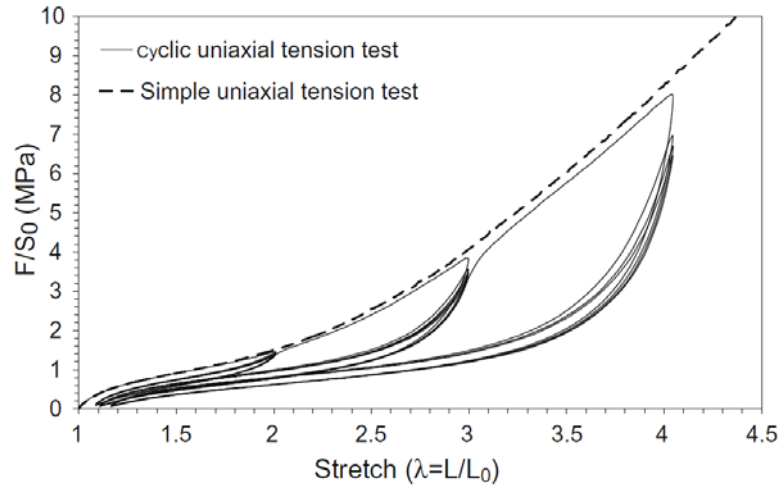
**Fig. 1.** Stress–strain responses of a 50 phr carbon-black filled SBR submitted to a simple uniaxial tension and to a cyclic uniaxial tension with increasing maximum stretch every 5 cycles.

- Most of the softening, which is characterized by a lower resulting stress for the same applied strain, appears after the first load.

- After a few cycles (values up to 10 are reported in the literature depending on the material nature), the material responses coincide during the following cycles, aside from a fatigue effect.

- The softening appears for stretches lower or equal to the maximum stretch ever applied.

- When the extension exceeds the maximum extension previously applied, the material stress‑strain response returns on the same path than the monotonous uniaxial tension test stress‑strain response after a transition, which increases with the amount of strain.

- The softening increases progressively with the increasing maximum stretch

16

The Mullins effect continues to be a source of discord between reported material properties and effective ones. When the 100% and 300% moduli for an elastomer are included in test data, they usually are defined to be the stress required to achieve 100% and 300% elongation of a material *on the first cycle*. These values are each only meaningful so long as the material is not stressed above them, and they provide no information as to how to interpolate between or below them. Unlike the modulus of elasticity for metals, these are single data points, isolated and unrelated.

Another obstacle to material candidate selection is the problem of hysteresis. For one reason or another, mechanical energy lost under fully reversed cyclical loading does not usually appear on manufacturers' reports. Perhaps the use of polyurethane in energy storage is not common enough to warrant cyclical testing, especially given the time consuming nature of stress-strain tests on high strain materials. Whatever the reason, finding a material with optimum hysteresis properties is currently more guesswork than not. Some manufacturers list compression set and tensile set among their material properties. However, as will be shown below, these static tests reveal very little about the cyclical behavior of polyurethane. As a result of these problems, it was decided that instead of a drawn out search for the optimal elastomer, a survey of several readily available polyurethanes would be performed, and the most adequate of these would be used to establish a baseline. The majority of work undertaken would be to establish accumulator designs for maximizing the performance of a given polyurethane as a strain energy accumulator. This way, as further advances occur in the polymer industry, these advances would directly result in increases in accumulator performance.

Six formulations of polyurethane were purchased from McMaster-Carr and three formulation samples were provided by Lubrizol, a specialty chemicals manufacturer and industry member company of the CCEFP. From McMaster-Carr, a durometer selector pack was purchased, which included sheets of black polyurethane of durometers 40A, 80A, 90A, 95A, and 75D (listed in order of increasing hardness and reported tensile strength). Additionally, amber sheets of 90A polyurethane were also purchased. MSDS records were provided which listed Pleiger Plastics Company as the manufacturers of the polyurethane sheets. After investigating several manufacturer reports on Matweb online material database, we selected Lubrizol TPUs Estane 58325 and 58280 for investigation due to their high reported elongation, tensile strength, and rebound. Later, after conferring with a technical representative, samples of Estane 58238 were also acquired and tested. Later still, additional hollow tubes and solid bars of black polyurethane 90A durometer were obtained from Polyurethane Plastics Corporation, again through McMaster-Carr.

CHAPTER 3

**Material Selection Prototype**

1.  Motivation and Construction

Even among polyurethanes, great disparities exist between formulas, both in terms of strength, maximum extension, and mechanical damping. Furthermore, these properties are independent. No firm rules exist relating the three, so while one formulation may have twice the strength of another, their hysteresis properties may be identical or very dissimilar. Since hysteresis is not a property commonly reported by manufacturers or distributors, cyclical testing of a wide array of polyurethanes was a necessary step for determining the span of readily available candidates.

In order to narrow down the selection of available polyurethane formulas, a prototype was designed that would allow for simple, repeatable testing and exchanging of specimens of various stiffnesses. A rounded square and twelve hole pattern was used to laser cut specimens from sheets of polyurethane. These specimens could then be securely mounted as a diaphragm blocking the inlet to the device's clear expansion chamber. Tie rods were used to ensure an appropriate magnitude and distribution of clamping force as well as to prevent the diaphragms from shifting or slipping during testing. Pressurized nitrogen was piped through a regulator and ball valves into the cavity behind the diaphragm. Pressure was recorded via a Kulite XTL-190-5000A pressure transducer with analog filtering and amplification. The expansion chamber was filled with water and let

through a tube to a vertical water column inside a graduated cylinder. This allowed the quick measurement of displaced volume regardless of the shape the diaphragm took and without electronics or flow sensors. Nitrogen was allowed to enter the device incrementally while pressure and volume displacement readings were recorded. Measurement continued as the nitrogen was vented incrementally so that both charging and discharging of the accumulator could be recorded.
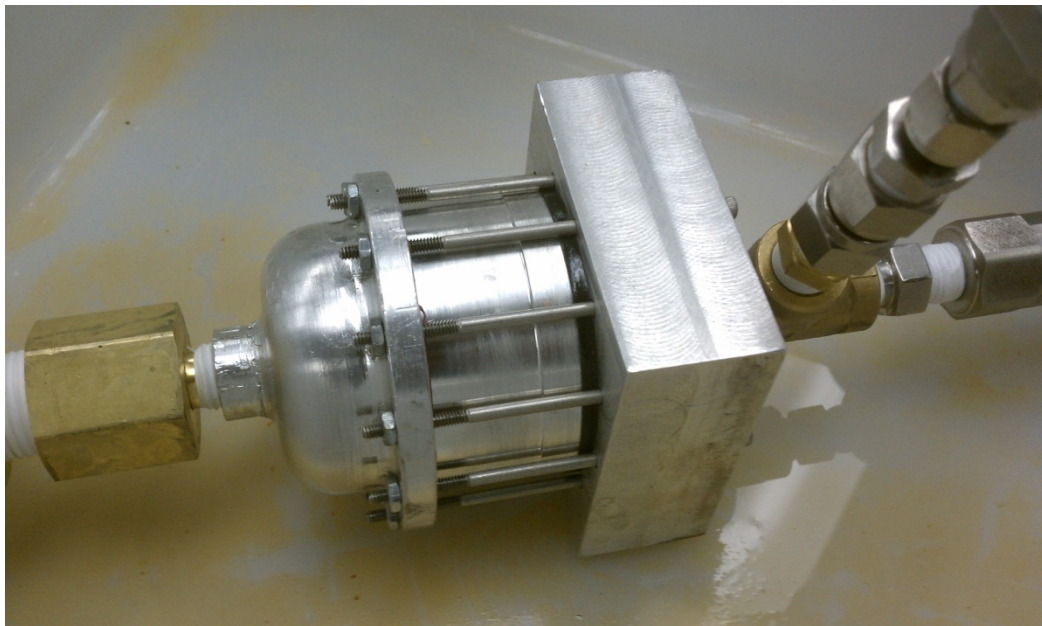


Figure 5 Material Selection Prototype

Each specimen was inflated to a volume change of about 60 mL. For the given setup dimensions, a volume change of 50 mL behind the diaphragm can be approximated by a hemisphere of radius equal to the chamber radius (1.125") whose surface area (7.9") is nearly double that of the uninflated diaphragm (4.0"). The average strain in the diaphragms could therefore be estimated between 100% and 130%. After about 60 mL of inflation, the contact between the inflated diaphragms and the expansion chamber

walls was judged to be significant and might have introduced additional complexities into the diaphragm stress profiles. For this reason, as well as pressure limitations of the pneumatic setup, the prototype was capped at about 60 mL of displacement. For comparison, some diaphragms were purposefully overinflated to failure into an empty expansion chamber. Though the failure displacement was not measured directly,

Because of the geometric complexity of a diaphragm being inflated into a cylindrical chamber, steps were taken in order to isolate geometric effects from material selection effects. Diaphragms were cut from sheets ranging in thicknesses from 1/16" to 1/4". By varying the diaphragm thickness/diameter ratio, the various formulations could be compared under multiple load conditions, thus ensuring a candidate did not outperform the rest due to some hidden geometric preference.



Figure 6 Post-Test Diaphragms

A further advantage of the material selection prototype was that it allowed multiple diaphragms to be stacked in series—with a thin, water filled cavity between them—in order to examine the effectiveness and efficiency of the Diaphragms in Series configuration (described in more detail in chapter 5).  Figure 6 contains two 1/16" diaphragms in series with an 1/8" acrylic spacer between them, which ringed the water filled cavity.


## 2.  Results


Trapezoidal integrals of pressure-volume data were taken in order to calculate energy stored during inflation and percent energy lost in the round trip.  The area under a pressure-volume charging curve, divided by the mass of the diaphragm, gives a benchmark for comparing the energy storage densities of the materials.   The area circumscribed by the charging/discharging cycle (henceforth called the hysteresis loop) gives the amount of energy lost by system inefficiencies.  Dividing this into the total energy stored during charging gives the percent energy loss.  Figure 7 shows the pressure-volume profiles of many of the tested diaphragms as well as their percent energy loss.  Figure 8 shows this information in chart form as well as the energy returned by each diaphragm per unit mass of the diaphragm.  These figures of merit, described above in chapter 1 section 3, were used to compare the candidate materials non-dimensionally.
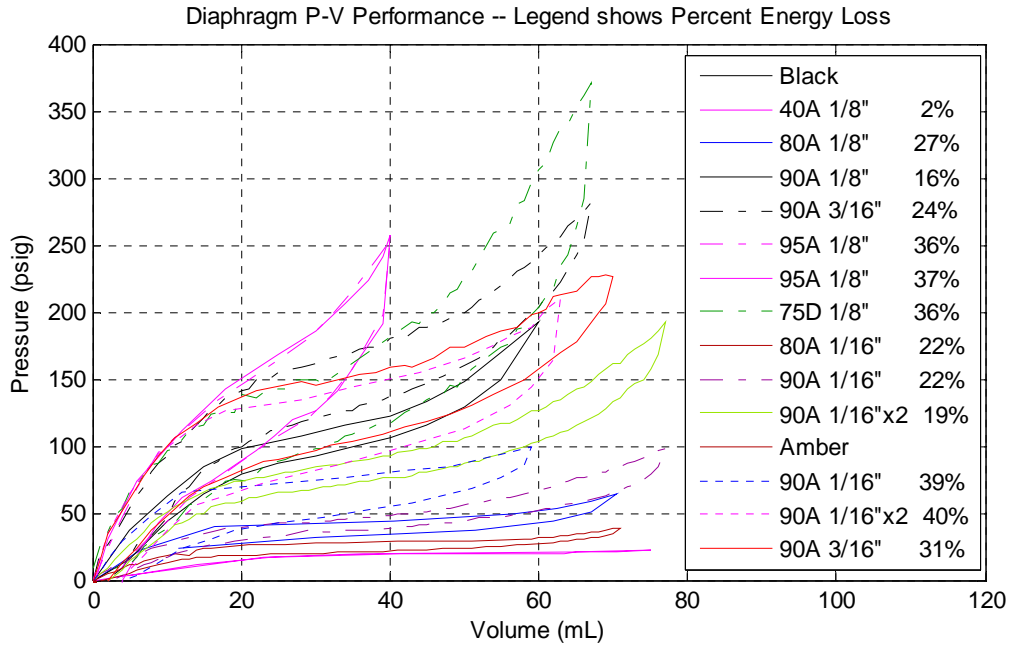
Figure 7 Diaphragm Comparison Graph
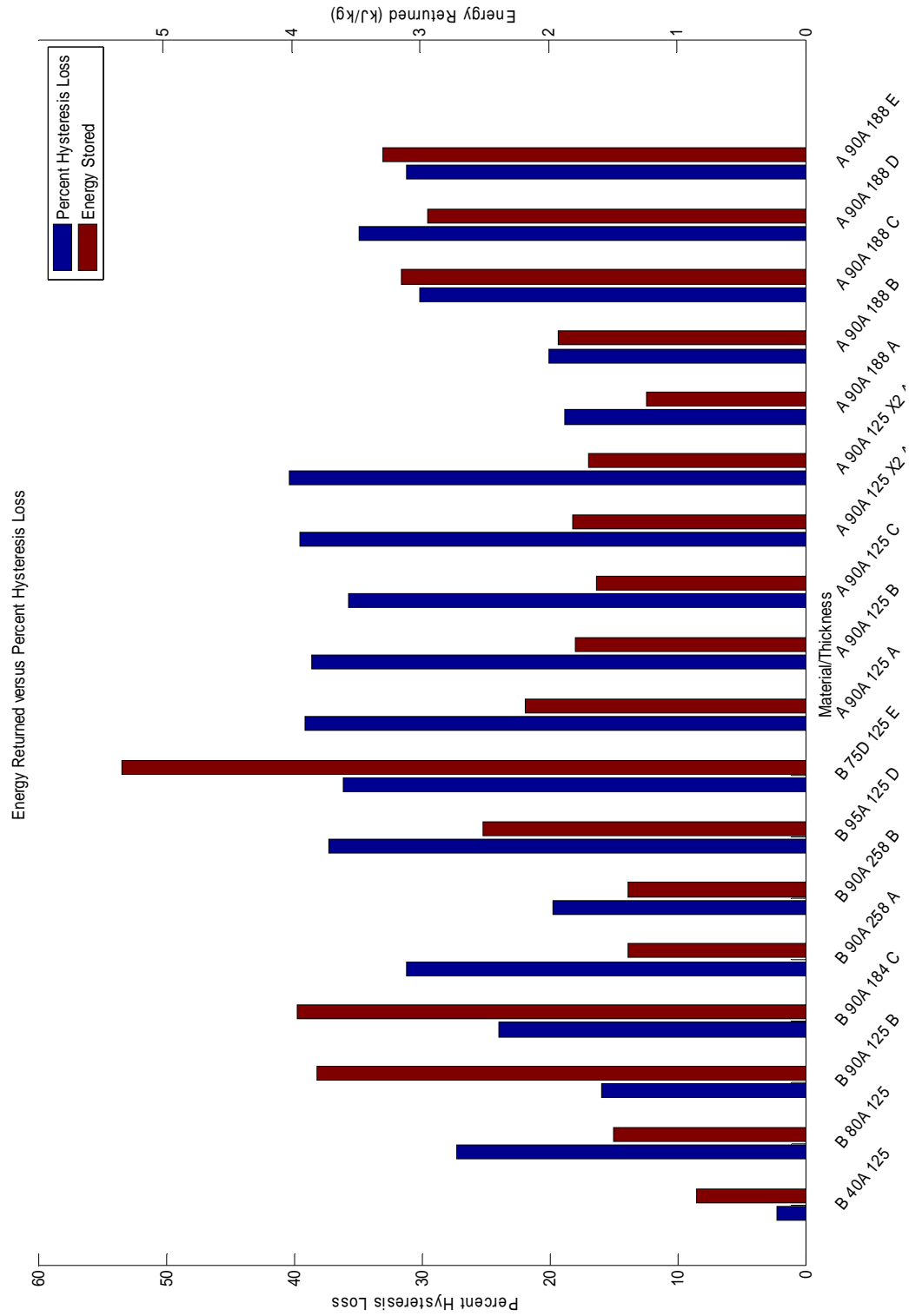
Figure 8 Diaphragm Energy Returned Per Unit Mass

## 3.  Conclusions

At all thicknesses, black polyurethane greatly outperformed Lubrizol Estanes and amber formulations in terms of percent energy loss.  A comparison of all of the candidates shows 75D and 90A to lead the rest in terms of energy storage density. Comparing the areas under their discharging curves—the energy returned per cycle—and dividing by their respective masses, 75D was capable of returning 38% more energy than an equal weight of 90A, but the percent energy loss (36%) was more than double that of 90A (16%).  In practice this means that for a fixed accumulator weight—which assumes that weight is the limiting factor—an undersized 75D accumulator would be able to absorb enough energy to return more than an equally small 90A accumulator.  However, if the accumulators were large enough to absorb all of a vehicle's kinetic energy—which assumes that weight is not the limiting factor—a 90A accumulator would be able to return up to 84% of the energy, while a 75D accumulator would only be capable of returning 66%.  Because of its higher efficiency, 90A black polyurethane was selected for continued study.

Despite being the leading performer, 90A displayed an energy density of merely 4 kJ/kg, a small fraction of the energy density projected by calculations based on reported strength and extension values.  With an ultimate tensile strength of 5500 psi and a maximum extension of 600% strain, the energy density should have been much higher. Even operating at half the $U_{ts}$, the energy density should be on the order of 19 kJ/kg, not 4. The reasons for this reduction in effective energy density are twofold, but both reasons stem from the geometry of the prototype.

First, diaphragms in inflation tend to become spherical as they grow. Both the cylindrical expansion chamber and the adjacent diaphragm in a series prevent the diaphragm from expanding naturally. The cylinder wall forces the diaphragm into a more complex domed-cylinder configuration as it contacts the wall while an adjacent diaphragm prohibits even this much expansion since direct diaphragm-to-diaphragm contact is undesirable.

Second, the transition from planar sheet to hemisphere results in large, negative bending moments throughout the dome as well as concentrated, positive bending moments along the clamping ring. The negative component of this bending moment, when superpositioned on top of the tensile hoop stress causes a gradient in the strain energy stored throughout the diaphragm. Strain on the inside surface of the diaphragm is considerably lower than that along the outside surface. Depending on the thickness of the diaphragm, the magnitude of this strain gradient can be on the same order as the average strain in the diaphragm. The end result here is that much of the diaphragm material is storing significantly less energy than it is capable of storing.

CHAPTER 4


**Pure Tensile Testing**


1. <u>Motivation</u>


In order to investigate the disparity between expected and observed energy densities, a setup was needed to test the stress-strain properties of the candidate material—polyurethane 90A black—under optimal strain conditions, uniform tensile loading. In addition, it was believed that although increasing loading strain up to a point would cause an increase in energy density, overstraining beyond this point would cause degradation of the material, significantly lowering its storage capabilities over time. Because precise strain is trivial to calculate in uniform tensile loading, the optimal loading strain could be determined by cyclically straining multiple samples to various maximum stresses or strains. This data would serve as a target goal that any future prototypes would seek to approach.


2. <u>Bucket testing</u>


*2.1 Construction*

Because of the high elongation of elastomers, traditional tensile testing machines—which specialize in tiny movements at high loads—seemed ill suited for quickly acquiring data for multiple samples over many cycles. Additionally, it was

desirable to test the properties of the material over a range of strain rates in order to determine if its energy density or hysteresis properties were adversely affected by either gradual or rapid straining. To this effect, a setup was created that would allow for a strain rate ranging from approximately 5-50% strain per second, estimated from the total strain range (about 300% extension and 300% relaxation) and time to completion (between 12 and 120 seconds).

Dog bone shaped samples were laser cut from 1/8" sheets and suspended from a table mounted c-clamp. A bucket was suspended from the other end of the samples and a gage length each sample was marked with paint and measured. As iron weights were loaded smoothly into the bucket, the extended gage length was measured with calipers, and both weight and length were recorded. Measurement continued as weights were removed incrementally, completing the hysteresis loop. For each cycle in a given set, the same maximum load (and therefore stress) was used. In one set, enough weight was used to stress the material to 1650 psi (about 30% of its Uts). In another set the stress was set at 2400 psi (about 44% of Uts). Energy storage density was calculated for each cycle in both sets by dividing the integral of the stress-strain curves by the initial volume of the gage length.

*2.2 Results*

Both sets of testing showed significantly higher energy storage density than the diaphragms in the material selection prototype. The 1650 psi set averaged at 9.5 kJ/kg, while the 2400 psi set averaged at 12.7 kJ/kg. The 1650 psi averaged 16% energy lost per cycle while the 2400 psi set averaged at 18%.
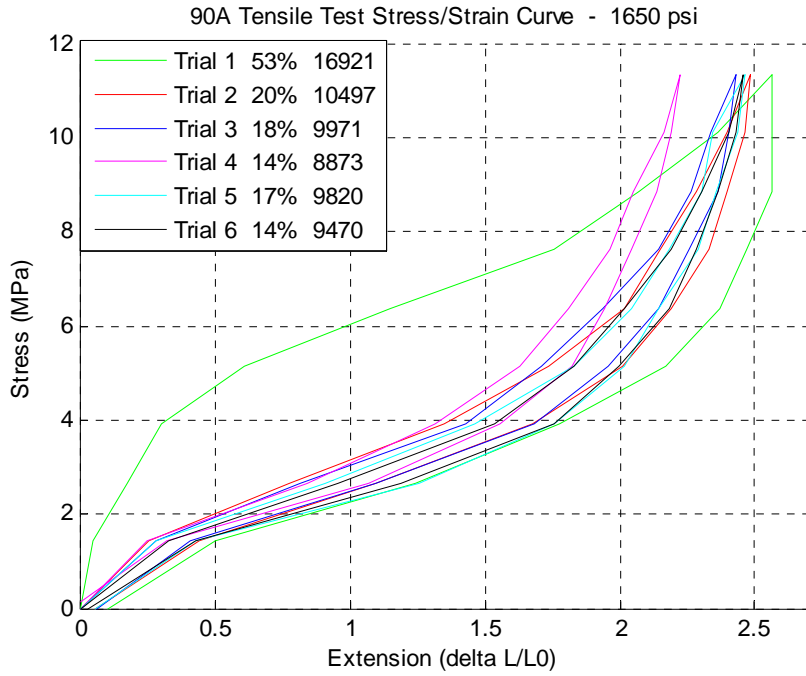
Figure 9 Bucket Tensile Testing Sample 1
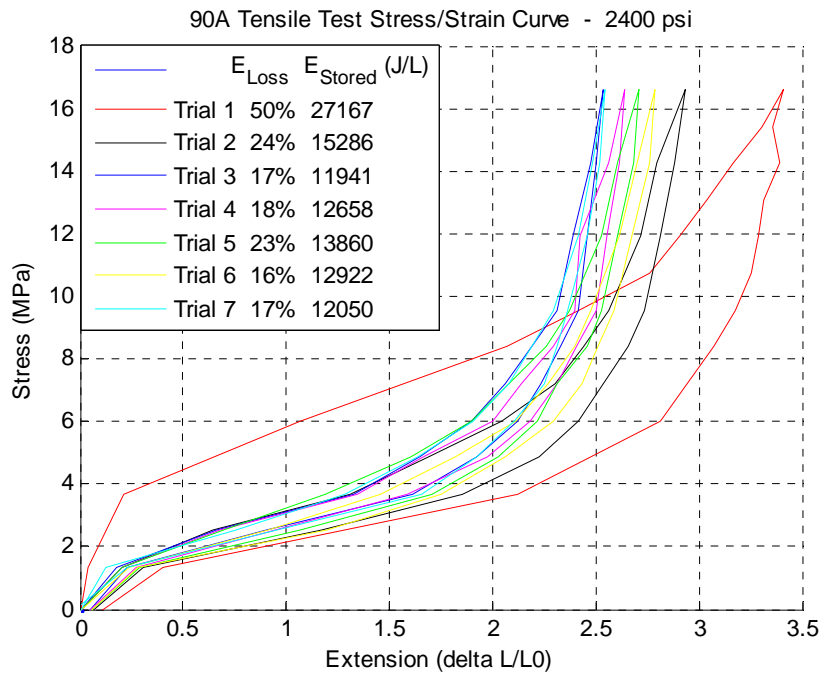


Figure 10 Bucket Tensile Testing Sample 2

*2.3 Conclusions*

During this testing, three unforeseen complications arose which limit its effectiveness for producing precise, quantitative results. First, in order to add and remove weight to the device quickly and simply, discrete iron weights were used. Because the resolution of these weights is low, the step size of the test was necessarily quite large, with less than a dozen steps from zero load to maximum load. Additionally, while effort was taken to load each weight smoothly, any impact forces resulting from the weights shifting—an artifact of the crudeness of the setup—could throw off the behavior of the polyurethane. Since the strain of the elastomer is not 100% efficient, a sample stretched to an equilibrium length by the weight of a given load would settle at a longer equilibrium length if the same weight was loaded with an additional portion of kinetic energy. Finally, because no adhesives could be procured which bond well with polyurethane, extension of the elastomers had to be measured with calipers rather than contact extensometer, which lowered the precision of strain measurements and increased measurement time. After the first two cycle sets, these drawbacks, coupled with the promising energy densities displayed in the results, warranted the switch to more rigorous testing.

## 3. Machine testing

*3.1 Setup*

Now that it had been shown that a tensile stress of 2400 psi was significantly preferable to a stress of 1650 psi, more precise testing was required to further narrow the

band of target load.  This time, in an effort to increase the measurement precision and
repeatability, larger samples were cut and tested in an automated tensile test machine.
Initial gage length was measured, and extension and force load data was recorded via
software.  Specimens were stretched cyclically on average nine times with each cycle
taking an average of 5 minutes to complete.  Gage length measurements were updated
after a brief rest period following each cycle.  The first specimen was always stretched to
a load force corresponding to 2100 psi, the second specimen to 2400 psi, the third to 2850
psi, and the forth to 2500 psi.



Figure 11 Post-Test Tensile Specimens

*3.2    Results*

For every specimen, the first cycle was significantly less energy efficient than any
of the following cycles.  This Mullins effect, described in chapter 2 section 2, was
expected and observed in all cases.  For all but the 2850 psi specimen, the amount of
energy stored per cycle settled after about four cycles.  The standard deviation for their
energy storage was +/- 2% of the average for the specimen.  The 2850 psi sample by
contrast had a standard deviation of +/- 10% even after the first four cycles.

31

Figure 12 Machine Tensile Results Sample 1
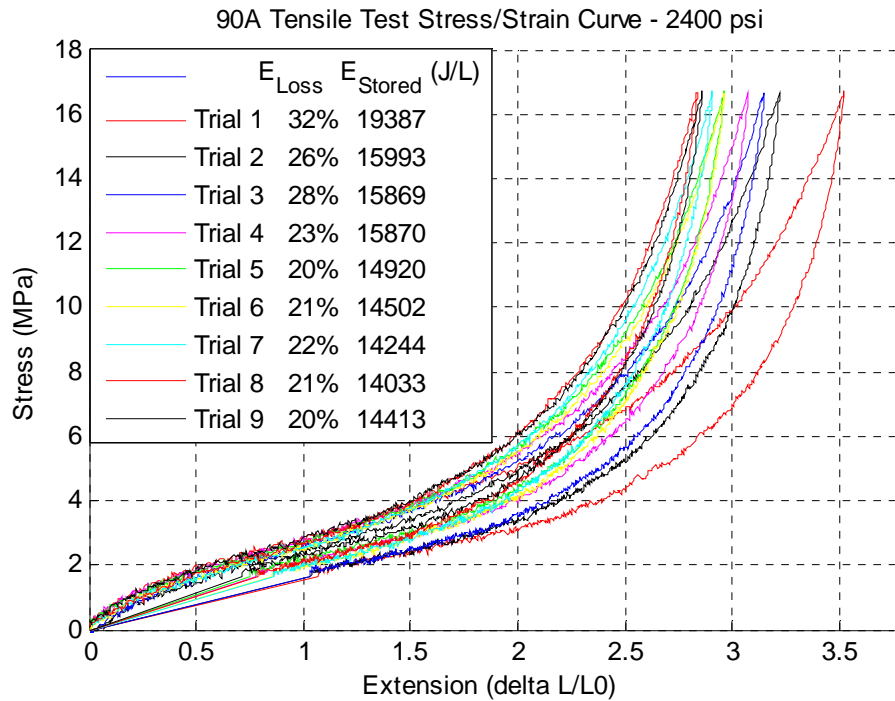


Figure 13 Machine Tensile Results Sample 2
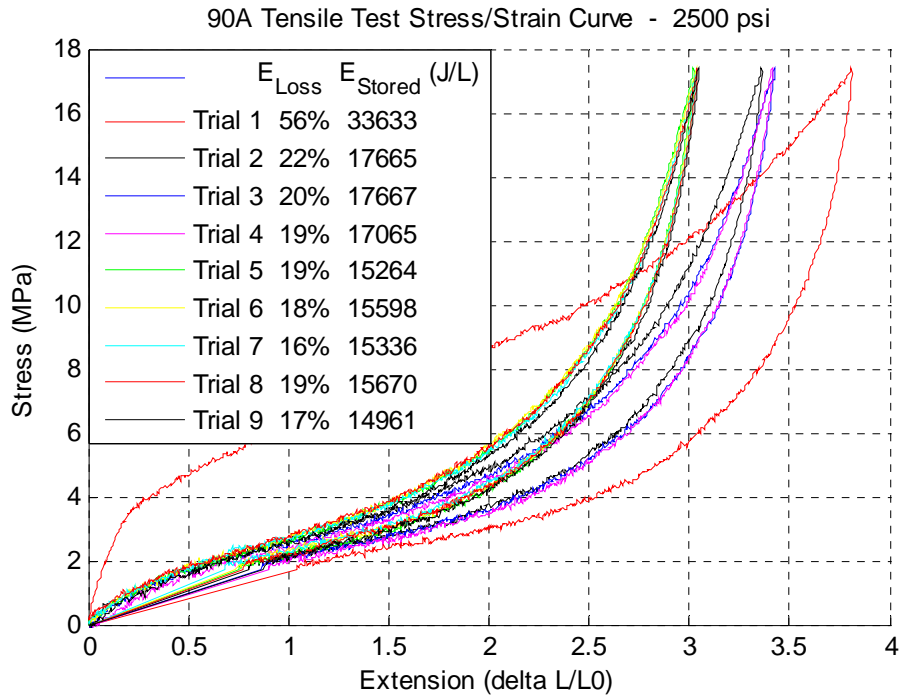
Figure 14 Machine Tensile Results Sample 3
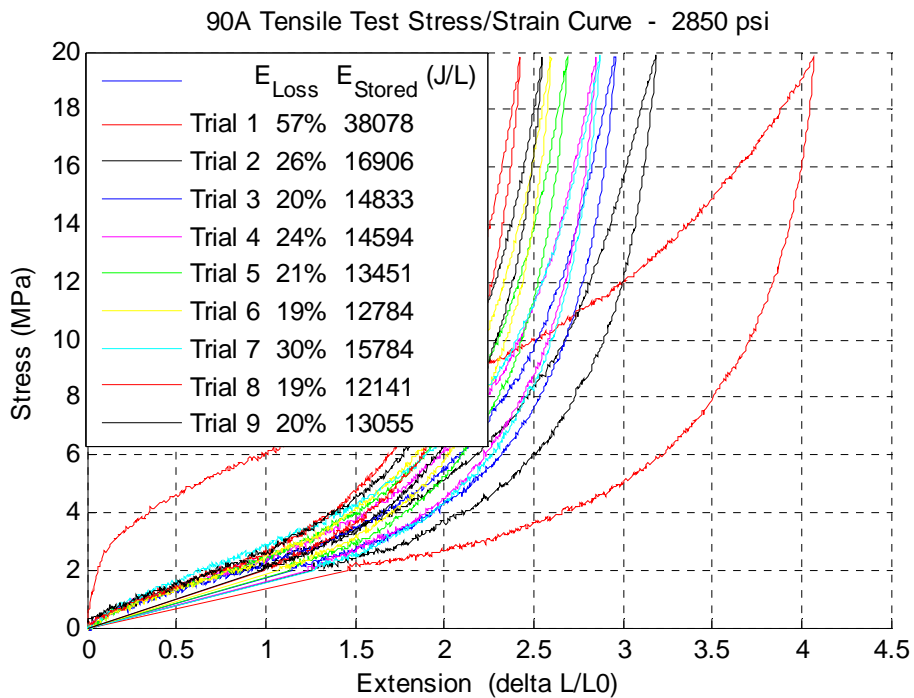


Figure 15 Machine Tensile Results Sample 4

33

Hysteresis percentages also settled within four cycles, again with the exception of the 2850 psi sample. Average energy densities and hysteresis losses are summarized below.

Table 1: Tensile Test Results

| $\sigma_{max}$(psi) | 2100 | 2400 | **2500** | 2850 |
|---|---|---|---|---|
| $e_M$ (kJ/kg) | 13.8 | 14.4 | **15.4** | 13.4 |
| $E_{Loss}$(%) | 20.0 | 20.8 | **17.8** | 21.8 |
| St. Dev. (%) | ± 0.8 | ± 0.8 | ± 1.3 | ± 4.7 |

*3.3    Conclusions*

As expected, the average energy density of the chosen polyurethane increased as a function of the maximum loading until a certain point where it then decreased. At 2500 psi loaded per cycle, the energy density was at a maximum while the energy losses were at a minimum. When stretched beyond this limit to 2850 psi per cycle, the performance deteriorated. It is possible that straining beyond a certain limit causes irreparable damage in each cycle, accumulating at a gradual but noticeable rate. While comparisons can be drawn between fatigue failure and the observed behavior, this phenomenon should not be oversimplified. Overloading a hyperelastic material actually makes it significantly softer at low strains while causing it to later stiffen, reaching the higher stresses at lower strains than specimens not subjected to overloading. Both phenomena are detrimental to energy density, since an ideal strain energy storage material would have a near infinite modulus at zero strain and a near zero modulus at other strains.

Regardless of the underlying cause, overloading should be avoided in any accumulator design.  It is unclear whether or not the optimal stress loading found for this particular polyurethane formulation can be used to generalize about optimal stress ranges for other elastomers.   However, in any further testing of this formulation, the target maximum uniaxial tensile stress can conclusively be set between 2400 and 2500 psi.

CHAPTER 5

**Candidate Geometries**

1. Target Metrics

*1.1    Pressure-Volume curve shaping*

One of the primary concerns when designing a hydraulic strain energy accumulator is the shape of the fluid pressure-volume curve during charging and discharging. As stated in equations (8) and (10), the energy density of the accumulator depends heavily on the average fluid pressure. Because of the large deformations involved in a strain-energy accumulator, the mechanical advantage (or disadvantage) that the working fluid has on the elastomer can vary greatly throughout the process. Changes in elastomer shape and aspect ratio can increase or decrease the surface areas exposed to fluid pressure. The maximum pressure of the device is limited both by the properties of the material and the properties of the hydraulic pump-motor, and the integral of the pressure-volume curve is equal to the total energy being transferred by the working fluid. Therefore, the average fluid pressure, and the corresponding total volume of fluid required varies as a function of the pressure-volume curve shape. Since the stress-strain curve of a high deformation hyperelastic material has a low average stress, it is important to maximize the mechanical advantage of the working fluid as the stiffness of the material increases and minimize this advantage along the low stiffness region. This

process, henceforth called "curve flattening," increases the average power density (and total energy density) of the working fluid by raising the average fluid pressure.

In addition to the role that curve flattening has on system energy density, it can also play an important role in the matching of accumulator load to desired output effort. Any system of regenerative braking must be controlled in such a way as to provide desired levels of torque to the drivetrain both in charging and in discharging. While the final onus of this effort matching must be handled by some form of variable transmission, the job of the transmission can be greatly simplified if the effort profile of the accumulator is flattened. Because torque requirements are in general dependent on user-input and not accumulator state, a highly varied effort profile can only add to the burden of transmission, not lessen it. Therefore, the ideal effort profile for a regenerative braking accumulator is a constant value function, a far cry from unmodified stress-strain profiles of hyperelastic materials.

## 1.2    *Maximize material utilization*

While pressure-volume curve flattening is important for increasing the power density of the working fluid, maximizing the energy storage density of the device is also largely dependent on maximizing material utilization. Whenever some portion of the elastomer is stressed less than the rest, this underutilized material directly reduces the overall system energy density. It adds to the overall system volume as much as the rest of the elastomer, but it stores less energy, thereby lowering the average material energy density. In an ideal accumulator, when the system is fully charged, all of the elastomer

will share the same strain energy, even if the stress configuration is not necessarily uniform or symmetric.

*1.3      Minimize dead-space volume*

Another important contribution to the total energy storage density of a hydraulic strain energy accumulator is dead-space volume. This volume includes the entirety of the discharged accumulator volume minus the volume of utilizable elastomer. Pressure vessel containment, elastomer gripping length, mounting equipment, and pockets of intermediary fluid all contribute to dead-space volume. Some of these contributions serve necessary functions in any working accumulator, but minimization of dead-space volume as a whole must be thoroughly addressed in any accumulator design and implementation.

2.  Simple Bladder

One of the first accumulator designs, an elastomeric bladder, inflated from within, exemplifies the tradeoff between the three primary design motivations mentioned above. This design was first examined for its superior P-V curve shaping properties. As a long, narrow bladder is inflated from within, it balloons outward locally, a bubble forming at its weakest section. At some later strain state, the radial expansion of the bubble slows to a halt, and the bubble begins to propagate along the length of the bladder.

To explain this phenomenon, one can first examine the cross-sectional slices at various planes along the length of the bladder at a point in time when the bubble has

begun to propagate. Each cross-section shows a hoop-shaped area of elastomer circumscribing a circular area of working fluid. Cross-sections taken at the narrow end of the bladder have a relatively small area of working fluid contained by a ring of relatively unstrained elastomer. Cross-sections taken at the apex of the bubble have a much larger area of working fluid contained by a ring of highly strained elastomer. Cross-sections along the gradient between the two regions form a continuum, both in terms of fluid area and material strain.
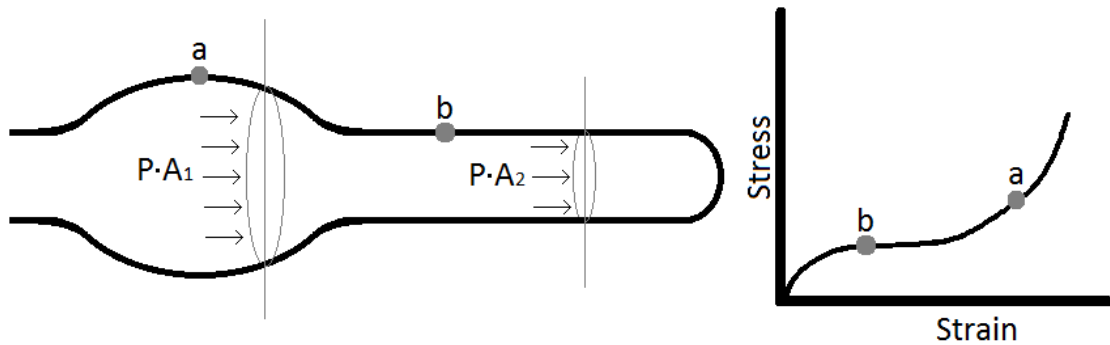


Figure 16 Bubble Propagation Phenomenon

The strain in each cross-section can be loosely approximated as being proportional to the radius of the fluid area. This is because the elastomeric ring forms a perimeter around the fluid, with its arc length (and therefore hoop strain) being proportional to the radius. The free body load of each cross-section, the force summation which the axial stress of the elastomeric ring must oppose to maintain static equilibrium, is a product of the current fluid pressure (uniform throughout all cross-sections) and the fluid area, because the fluid area is equivalent to an axial projection of the sectioned off region of the elastomer back on the sectioning plane and is therefore equal to the dot

product of the pressure vector and the positive longitudinal axis, integrated over the sectioned off region—the free-body load force summation.

Since the strain in the material is linearly proportional to the radius, while the fluid area is proportional to the square of the radius, the pressure required to achieve a given strain (corresponding to a given radius) is a product of the corresponding material stress and the radius inverse. The end result of this phenomenon is a curve flattening effect which comes from the increasing mechanical advantage that the pressure receives along the bubbled region.

While the simple bladder design presents a significant opportunity for P-V curve shaping, it places the remaining two design metrics in direct opposition to one another. As stated before, the cross-section of the bladder design consists of an o-shaped ring of elastomeric material. Unstrained, this material has an initial inner circumference and outer circumference which are related by some initial ratio. As the bladder is inflated, however, this ratio does not remain constant. Like any thick-walled pressure vessel, the interior surface experiences the maximum stress, with the stress decreasing along the radius to a minimum at the external surface. The magnitude of this stress gradient depends directly upon the initial ratio of circumferences. The closer the circumferences (the thinner the wall), the smaller the stress gradient. At the other extreme, where the inner circumference is very small by comparison, the stress gradient approaches the magnitude of the maximum stress, and the stress along the outer surface approaches zero.

By this reasoning, in order to maximize the material utilization—the second priority in accumulator design—one must choose a thin-walled bladder, with a circumference ratio close to one. This, however, poses a large problem in terms of the

third design priority, minimizing dead space volume. A thin-walled bladder must be filled with fluid before it begins to resist further fluid influx. The material feels no strain and stores no energy until it is filled to unstretched capacity. This entire volume of fluid, therefore, can be considered to be dead-space volume, volume added directly to the total system volume without any energy being stored. For a thin-walled bladder, this volume of fluid is much greater than the volume of the elastomeric walls. Consequently, if the volume of elastomer needed to store strain energy makes up even a small portion of the total accumulator volume—this is true in all cases where the energy density of the elastomer is not orders of magnitude higher than the power density of the working fluid—then the fluid needed to fill the thin-walled bladder will add a much larger volume to the accumulator as dead-space volume. This tradeoff between material utilization and dead-space minimization is the primary handicap of the simple bladder design. (Pedchenko 2011)

### 3. Diaphragms in Series

In an attempt to greatly reduce the problem of dead-space volume, a second design was proposed which composed of a set of elastomeric diaphragms stacked in series. Each diaphragm would have a thin film or layer of fluid separating it from its neighboring diaphragms in order to transmit forces between diaphragms without frictional losses from surface interaction. These diaphragms would form a barrier column of identical components which cooperatively resist influx of fluid from either direction. As the first diaphragm in the series attempts to balloon inward to

accommodate the working fluid, its separating layer pushes the next diaphragm to move in the same manner.  This behavior propagates instantly through the entire column, with each diaphragm experiencing approximately the same strain.  Since each diaphragm experiences the same strain, each one contributes the same pressure drop to the column.  With enough diaphragms stacked in series, enormous working fluid pressures can be built up, pressures ten times that which would rupture single diaphragms.  A prototype of this design was constructed and also used as the test rig for polyurethane candidate selection (see chapter 3).

The simplicity of this design belies both its effectiveness and its complications.  Simple discs of diaphragm material, dropped into a pressure cylinder, spaced apart by thin spacing rings and filler fluid, and clamped down on like a hydraulic sandwich, this design is simple to visualize and to assemble.  The problems begin to arise, however, once the device is put into actual use.  In the light of existing elastomer parameters, the problems compound and soon become intractable.

The first problem, while not entirely fatal, is worrisome nonetheless.  When diaphragms in series are inflated, the shape that they take consists of a hemisphere-like dome with an inflection ring around the base.  This shape is a marked departure from the initially flat disks, and contains therefore a significant amount of bending stress.  Bending in a diaphragm—much like that in a beam—creates an axial distribution of strain energy, with the magnitude of the distribution being related to the curvature of the diaphragm. The gradient adds to the strain energy stored in the areas of negative bending and relieves some of the strain felt by the areas of positive bending.  This causes some of the material to experience significantly more or less strain than the rest.

The second problem, while theoretically inconsequential, in practice proved to be insurmountable, given the range of materials currently available. As stated previously, the average maximum strain reached in these experiments was between 100% and 130%. This constraint was imposed not by material limits but by geometrical ones. Inflating the diaphragms beyond 130% caused them to contact the chamber walls more and more. Not only does this cause undesirable friction forces during the discharge phase, but also this geometry cannot be closely stacked and is therefore incompatible with diaphragms stacked in series. Theoretically, an elastomer with three times the stiffness and one third the maximum elongation of the chosen polyurethane would be well suited for operating in the 100% to 130% regime. However, no such materials have been found. For the chosen material, a cap of 130% maximum strain reduces the maximum strain energy density to about one third of its potential.

4. House-Grille Bladder

As testing was still underway for the diaphragms in series prototype, a third possible geometry was proposed in an attempt to combine the curve flattening effect of the simple bladder design with the close-packed series design of the diaphragms in series. Like the diaphragms in series, multiple planar layers of elastomer would be stacked with a thin separating fluid layer between them. However, by using long, rectangular sheets rather than circular discs, and by joining the sheets along their edges, a bladder is formed. The cross-section of this bladder looks like a grille, with vertical slits representing the fluid layers between the elastomer walls.
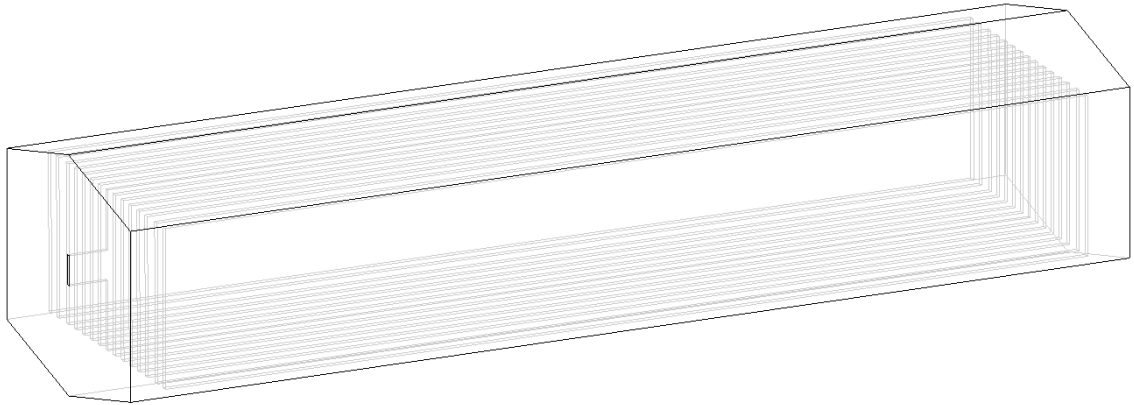
Figure 17 House-Grille Bladder CAD Model

The bladder is bilaterally and horizontally symmetric. The top half of the cross-section resembles a simple house shape, with identical pillars spaced along the ground 'floor' and a solid elastomer 'attic'. The slope of the 'roof' accounts for the difference in absolute pressure of neighboring chambers. The centermost chamber is at the highest pressure, with pressure decreasing in both directions with every chamber in the series.
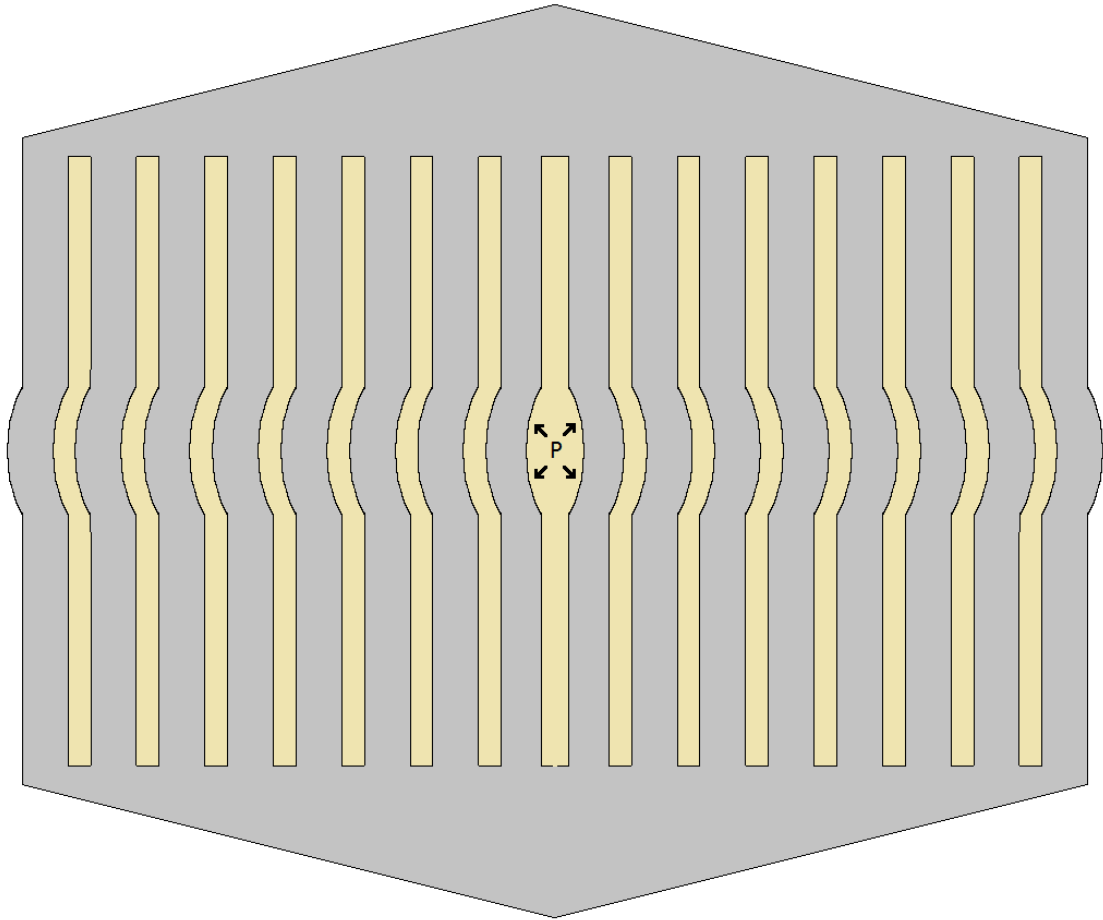
Figure 18 House-Grille Bladder CAD Model Cross-Section

The key distinction between the house-grille bladder and the simple, axisymmetric bladder lies in the uniformity of the layers. Imagine a thick-walled, axisymmetric bladder composed of several nested, thin-walled bladders. These bladders would form a series like that in the house-grille bladder and the diaphragms in series where each layer creates a pressure differential across it when stressed. The inner-most layer experiences the highest pressure, and the pressure between the layers decreases with every layer. In this case, however, the layers are not identical to one another. In particular, their circumferences are all different, and this difference prevents them from

uniformly sharing strain energy during inflation. The end result is very similar to a thick walled simple bladder, with the inner wall experiencing much more stress and strain than the rest of the material. With the house-grille bladder, each layer has the same initial height. They each strain in the same manner to the same extent, and as such they distribute the strain energy evenly, solving the problem of maximizing material utilization.

Because it uses fluid pressure, acting directly on the deforming surfaces, which deform in such a way as to increase the area upon which fluid pressure acts, the house-grille bladder would most likely retain the curve flattening capabilities of the simple bladder design. As fluid is pumped into the central chamber, the chamber should balloon outward horizontally at its weakest point, with the remaining layers mimicking this behavior. Like the simple bladder design, this deformation grants additional local mechanical advantage and promotes further extension at lower pressures.

The main problem with the house-grille bladder design is its complexity and high number of variables. In addition to the number of cavities and cavity heights, the overall bladder length, the cavity spacing, and even the slope of the 'roof' must be somehow optimized if the design is to be successful. In addition to sizing considerations, the complexity of the design poses a great many manufacturing conundrums. Rectangular cavities may require rounded corners to reduce stress concentrations. Fluid filled cavities must somehow be able to be filled with fluid after the elastomer is made, but they must also be sealable to very high pressures. Given the difficulty inherent in both shaping and in sealing polyurethanes, the house-grille bladder design quickly lost favor. Even a single stage of the device—a single rectangular chamber with rounded internal corners

and a sealed inlet port—proved difficult to prototype and leaked at relatively low strain values.



Figure 19 Single Stage House-Grille-Bladder Silicone Prototype

5. Rack and Roller

About the same time as the house-grille bladder design was put forth, a method was being investigated by which the mechanical advantage enjoyed by the simple bladder design could be obtained through kinematics as opposed to fluid power. The rack and roller design combines two simple mechanical concepts in order to provide a constant-force elastomeric accumulator load.

First, approximating an elastomeric cord as a series of infinitesimal springs in series, it can be seen that any given length of such a cord would provide the same amount of tensile force to its supports, given a set percent elongation. This holds true for all constant cross-section materials in tension. Tensile force is the product of area and stress. Stress is a function of strain only, which is not dependent on absolute length, but rather percent elongation.

47

Second, rotationally coupled wheels of different diameters have tangential velocities in equal proportion to the inverse of their diameter ratio. This means that a rotating wheel with a diameter of ten inches will have a tangential velocity one tenth that of a one inch wheel affixed to its axis. The rack and roller design combines these two effects by using a ratio of wheel diameters to fix the percent elongation in an elastomer cord while feeding more unstrained material into the growing stretched length.

Driven by torque from wheels or a drivetrain, a large driving gear rotates about a fixed axis with a small pinion fixed to its center (rotating at the same angular velocity). The driving gear engages a rack of length equal or greater to the length of an elastomer cord when fully stretched. The rack has one degree of freedom (it can only slide back and forth along its length) and has an anchor attached at one end which in turn grips one end of the elastomer cord, henceforth called the strained end. The cord is pinched at some point along its length in a no-slip manner by the above mentioned pinion and a passive, freely rotating roller, mounted to the accumulator housing. This region of cord, from strained end to pinch point is always held by a constant tensile force at a constant percent elongation, regardless of its actual length. Beyond the set of rollers, the free end of the elastomer cord hangs in a fully relaxed state.
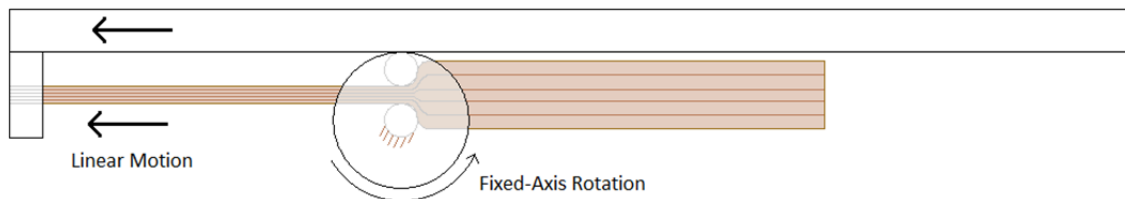


Figure 20 Rack and Roller Schematic

As the driving wheel turns, it forces the rack to move at its tangential velocity. This in turn pulls on the strained end of the stretched zone. Simultaneously, the pinion wheel turns at the same angular velocity, but the ratio of diameters causes the unstretched material to be fed at a much slower tangential velocity into the stretched zone. This ratio of velocities is fixed and therefore fixes the percent elongation of the material. Once energy stored in the accumulator needs to be recovered, a clutch mechanism will engage the driving wheel in reverse, and the rack and roller mechanism will return the stored energy in a constant torque manner.

The largest foreseeable caveat to the rack and roller design lies within the no-slip condition between elastomer and pinion. Essential to the design—as slipping of the elastomer allows energy to bleed from the system—this condition is nontrivial to achieve, particularly without the ability to cast complex elastomer shapes, like teeth on belts. Furthermore, the rack and roller omits completely the working fluid of a hydraulic regenerative brake. This removes some of the aforementioned advantages of hydraulics, and saves little space. While the uncharged accumulator appears to take up much less space than a bladder design as it lacks the reservoir of hydraulic fluid, in practice, the accumulator must claim additional space to provide room for the travel of the elastomer as it extends. By contrast, this space can be reclaimed by hydraulic braking systems by the integrated reservoir method. By using the travel volume of the elastomer to store the working fluid, the fluid reservoir is eliminated entirely as a separate volume cost.

In the end, the scope of investigation and experimentation that would be required on the subject of no-slip conditions of elastomers under high strain outweighed the net

benefits that a rack and roller prototype could be expected to produce.  As such, the design remains for now strictly theoretical.


## 6.  <u>Hinged Harp</u>


After initial tensile testing was performed on 90A black polyurethane, another kinematic design was put forth centered around the idea of pure tensile loading.  This idea utilizes trigonometric relations to define a variable moment arm through which a variable mechanical advantage scheme can provide curve flattening similar to that found in some of the above designs.

The hinged harp design consists of two rigid arms, joined at a hinge, with each arm having a roller wheel pinned to its free end.  These wheels roll along a fixed surface which forms a triangle with the two hinged arms.  Elastomeric cords, bars, bands, or sheets are strung from arm to arm, parallel to the rolling surface.  These cords form the strings of the 'harp' and resist the spreading of the arms.  In its unstretched shape, the arms form a narrow angle about the hinge (roughly 20 degrees).  The driving force— which could come from a hydraulic piston or some other mechanical linkage—pushes the hinge perpendicularly towards the sliding surface.  This motion translates through the rollers into a torque on each arm about the hinge. The cords provide a reactionary torque caused by stress in the elastomeric material.
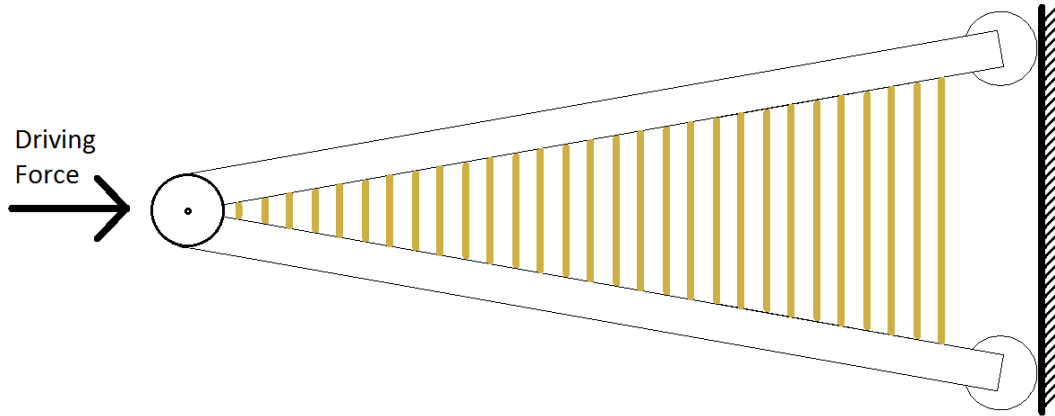
Figure 21 Hinged Harp Schematic, Relaxed Configuration

The stress on each cord is dependent not only on the number of cords (which is fixed) or the driving force, but also upon the moment arm which each cord 'sees' about the hinge. This moment arm for each cord is equal to the radial length from the cord end to the hinge scaled by the sine of the angle between the arm and the sliding surface (or cord). As the hinge angle grows from about 20 degrees to about 60, the mechanical advantage that each cord has diminishes by about 35%. The diminishment profile can be greatly influenced by the initial and final hinge angles, but these values are appropriate for flattening the stress-strain curve of the polyurethane in question. For a more easily calculated comparison, the uniaxial tension profile was simplified into a line of constant modulus, and then the driving force profile resulting from this variable mechanical advantage (the system effort profile) was calculated and plotted as a surface function of the initial and final hinge angles. This surface allows an observer to select a starting hinge angle based upon its corresponding force profile. Compared side by side with the linear (Hookean) force profile, the average force in a hinged-harp profile of equivalent maximum load is about 60% higher.
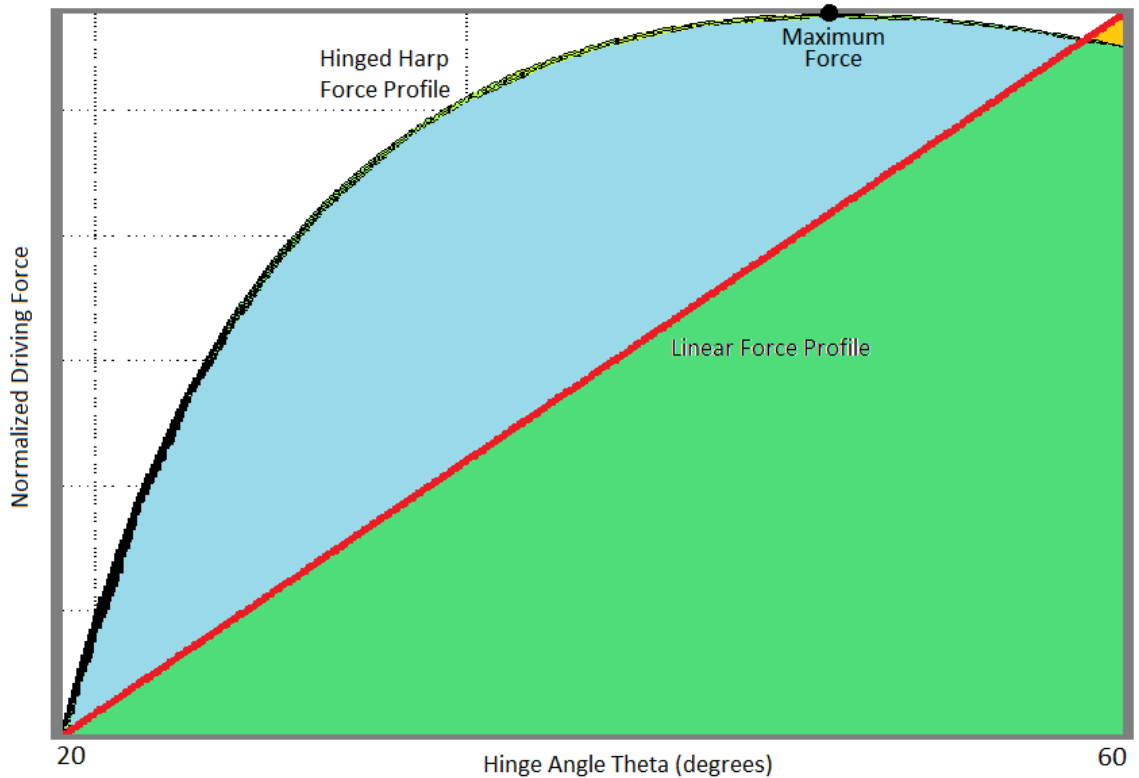
Figure 22 Hinged Harp Curve Flattening Simulation

As with the rack and roller design, the hinged harp design suffered from one major drawback. Because the extension path of the elastomeric bands was not contained within a reservoir of hydraulic fluid, the design cannot utilize the benefits of an integrated reservoir, namely, the volume through which *and* into which the elastomer strains directly adds to the dead volume of the overall system, dramatically lowering its volumetric energy density. Because of this, the gravimetric energy density of the hinged harp turns out to be significantly higher than its volumetric energy density. This drawback, once identified, coupled with the solid geometric understanding of the design's behavior and benefits, removed any demand for a prototype. If, however, the

design constraints for a particular hydraulic accumulator weigh gravimetric energy density more heavily than volumetric energy density, the hinged-harp design provides a simple and effective solution.


7.  Distributed Piston Elastomeric Accumulator (DPEA)


In order to incorporate both uniaxial tension and an integrated reservoir, a design was proposed in which a hydraulic piston was anchored to one cylinder end by an elastomer tether.  As fluid was pumped from the fluid filled side of the piston to the elastomer side, the tether would stretch and raise the fluid pressure by pulling backwards on the piston.  Since the tether stretched in the direction of the fluid reservoir, its trajectory adds no extra volume beyond the reservoir.



FIG. 2

Figure 23 Distributed Piston Accumulator Schematic from Patent App.


Further analysis of this approach revealed an added benefit that can be obtained when the tether ends fully engage either the piston or cylinder end.  In this case, the fluid pressure

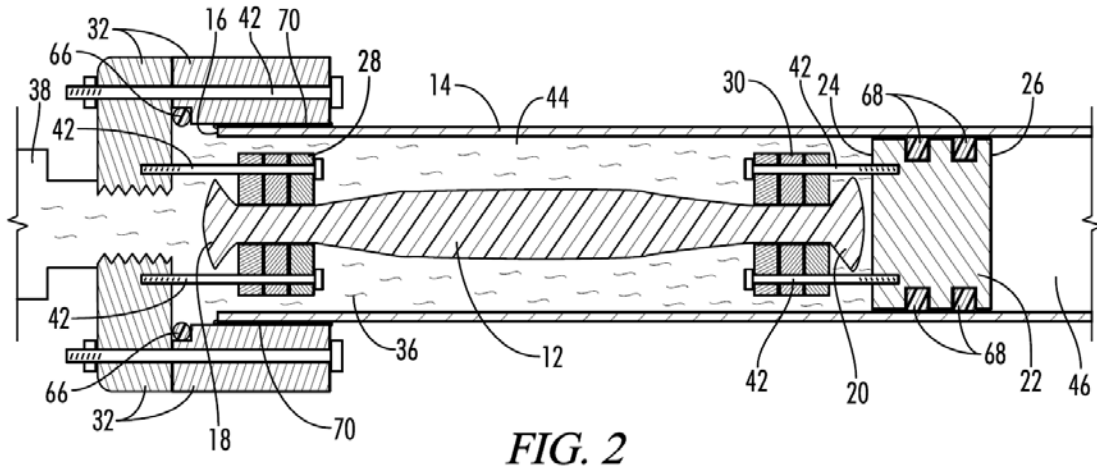can only act along the length of the elastomer and the small annulus of the piston to which it is exposed. When the elastomer is unstretched, its surface is primarily parallel to the cylinder axis and thus the force along the surface caused by fluid pressure has only a minute axial component. As the elastomer thins, however, it tapers down from where it engages the piston to some thinnest spot along its length. This taper, when viewed from a cross-section taken at the thinnest point, looks and acts like a secondary annular piston with a constant outer diameter and an inner diameter which shrinks as the elastomer stretches. The axial component of the pressure force acts along this taper so that the effective piston area increases continuously as fluid is pumped into the accumulator. This distributed piston effect naturally shifts the mechanical advantage of the fluid from very slight—in the case of a small annular piston—to very significant—in the case of a large distributed piston. Since the magnitude of this advantage shift is dependent upon the growth in piston area relative to initial piston annulus, it becomes more and more significant as the initial ratio of fluid volume to elastomer volume is reduced. Reducing the dead volume of fluid present in the elastomer chamber at zero pressure directly benefits the pressure-volume curve flattening effects of a distributed piston accumulator.

Another analogy that was developed for explaining the distributed piston effect comes from thinking of an elastomer section as springs in series. Figure 24 shows a series of springs, fixed at one end, with a piston at the end, and with thin plates in between each pair of joined springs. Force is applied to the piston end, equal to the annular force $F_A$ that the fluid pressure in a DPEA applies to the piston annulus. Next, additional forces are placed on a pair of adjacent plates, prising them further apart. In the case of a DPEA, because the magnitude of these forces is dependent upon the

deformation profile of the specimen along its axis, the forces increase to a point as the 'plates' separate, and then they shift to the next 'plate' in each direction as the thinned region propagates. This phenomenon is like an inverse to the phenomenon seen in the case of a simple bladder inflation. Instead of walls thinning to the outside, the diameter thins toward the axis. In either case, the cross-section of fluid grows locally as the material strains, increasing the mechanical advantage of fluid pressure.
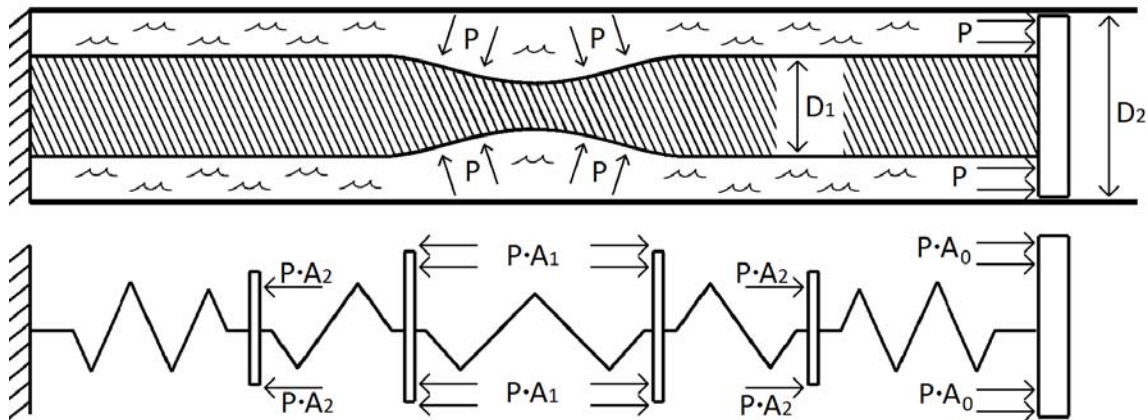


Figure 24 Distributed Piston Accumulator Spring Analogy

One significant problem with the distributed piston accumulator, which came to light during prototype testing, is that the fluid reservoir itself is inherently oversized in the case of conventional piston-cylinder technology. The nature of this problem can be most easily understood by examining an ideal version of a basic distributed piston accumulator. The entire cylinder encompasses a control volume divided by an infinitely thin piston into two chambers, one filled with reservoir fluid and the other filled with elastomer. The elastomer is bonded perfectly both to the cylinder end and to the piston. Fluid enters and exits the chamber through two ports, one located at the cylinder end on

the right, and the other located along the cylinder wall on the left. As fluid in pumped out of the right section, through a pump, and into the left section, the piston moves from left to right and the elastomer thins evenly everywhere except at the ends. At the ends it smoothly tapers to its original bonded area over an infinitely small axial distance.
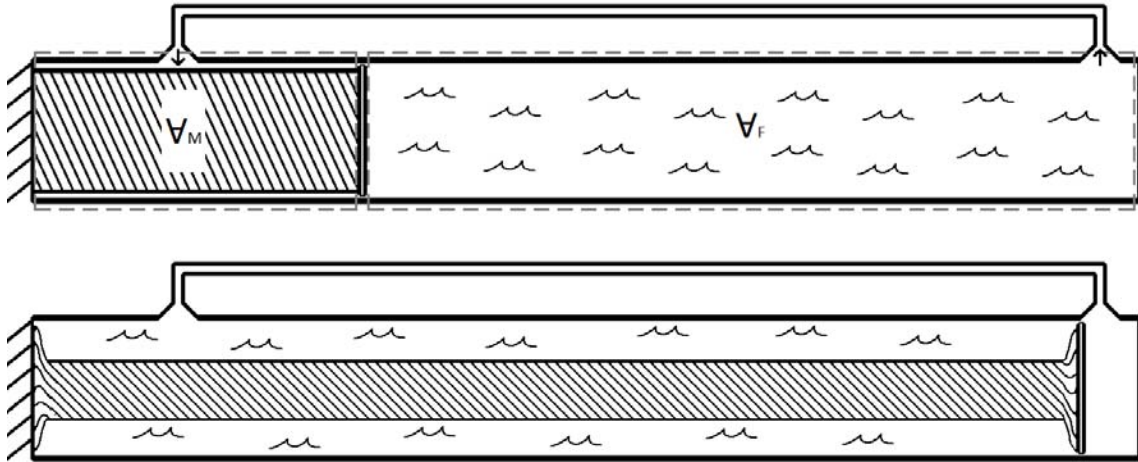


Figure 25 DPEA Volume Requirements

One can easily see from Figure 25 that in order to extend the elastomer to a given length, the piston must traverse the same linear distance. Since the area of the piston on the fluid side is always equivalent to the unstretched cross-section of the elastomer, the volume of displaced fluid $\forall_F$ is necessarily equivalent to the product of the initial elastomer cross-section and the change in elastomer length. Therefore, for a material strain of 300% to be achieved, fluid volume must be displaced equal to three times the initial elastomer volume $\forall_M$. The constant cross-section shape of the cylinder itself demands a reservoir—integrated or not—to be no less than the product of elastomer volume and maximum strain. Recall that energy density is the inverse of the sum of three

56

inverses and thus is impacted largest by the largest volume contribution. If fluid volume $\forall_F$ is necessarily three times larger than $\forall_M$, the energy density of the system in its entirety is at most 1/4th the energy density of the elastomer $e_M$.

This problem stems from a more fundamental one. When an incompressible material is strained, the volume remains constant. However, the control volume which envelops the material at any stage of its deformation is constantly changing shape. The overall envelope of a device containing this material must include the *union* of each of these control volumes. For a material of constant cross-section, fixed at one end, this union of control volumes is simple to compute. The material begins with an initial volume, area, and length $\forall_M$, $A_0$, and $l_0$. Add this volume $\forall_M$ to the envelope. From here, as the material is stretched, the free end of the material is constantly shrinking in area and moving normal to itself. Its perimeter traces a 3d surface which defines the boundary of the envelope as seen in Figure 26.
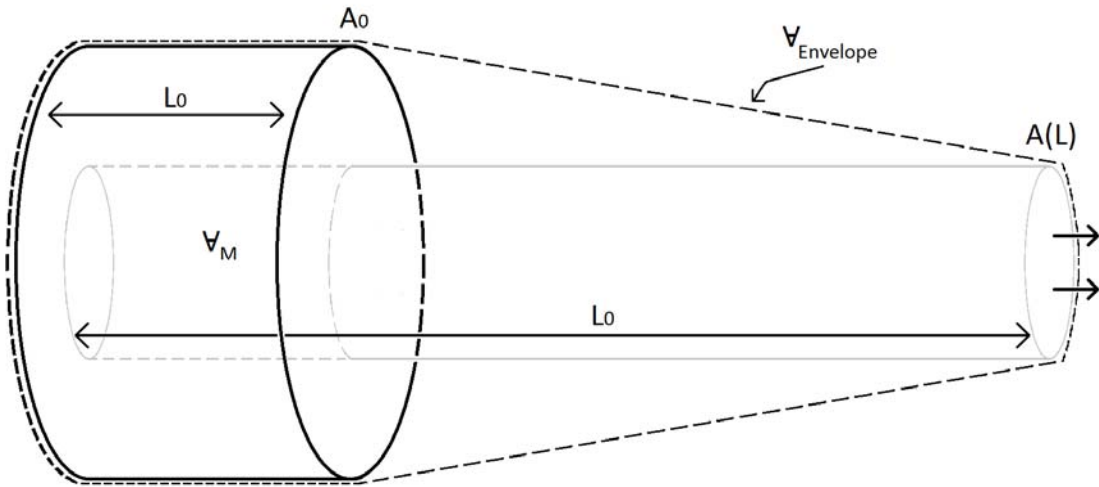


Figure 26 Volume Envelope of Uniaxial Extension

The entire material specimen is necessarily contained within this envelope. Therefore, the volume added to the envelope is equal to the integral of this area—which is a function of the length—over the change in length.

$$\forall_{Envelope} = \forall_M + \int_{l_0}^{l} A(l)dl \tag{13}$$

Because the material is incompressible, its volume is always equal to $\forall_0$, and therefore the area as a function of length can be calculated thus.

$$A(l) * l = \forall_M \tag{14}$$

$$A(l) = \frac{\forall_M}{l} \tag{15}$$

The equation for envelope volume then reduces to.

$$\forall_{Envelope} = \forall_M + \forall_M \int_{l_0}^{l} \frac{1}{l} dl = \forall_M\big(1 + ln(l) - ln(l_0)\big) \tag{16}$$

$$\forall_{Envelope} = \forall_M \left(1 + ln\left(\frac{l}{l_0}\right)\right) \tag{17}$$

For 300% strain, $l/l_0 = 4$, and thus $\forall_{Envelope} = \forall_0 * 2.39$. What this means is that uniaxial tensile strain accumulators are necessarily at least 2.39 times as large as their largest elastomer specimen. More practically, this means that they have, without a good bit of design trickery, less than 42% of the energy density of their elastomer. Still, 2.39 as large is smaller than 4, and 42% energy density is still higher than 25%. This

means that there is considerable room for improvement in the design of strain energy accumulators. For a single elastomer, complex loading schemes or housing designs can minimize the envelope volume. By using multiple elastomer specimens, their volume envelopes can be made to overlap somewhat, increasing the aforementioned 42% limit. With increasing complexity, however, come increasing secondary concerns. Grip length and size play larger rolls as the number of specimens increase. The role of friction between specimens or between specimens and container walls must also be taken into account. At the very least, such schemes will likely require the use of variable cross-section specimens, and as such they have been relegated to future work.

CHAPTER 6

**The Gripping Problem**

1.  Challenges

Perhaps the most challenging aspect in the design of a hydraulic energy accumulator is the management and application of forces to the elastomers being strained.  The concepts of mechanical advantage and strain energy distribution place extra burdens upon any such designs, but before either of these can be broached, a deceptively simple question must first be answered.  How can a device hold onto an elastomer?  The problem is inherently threefold, but is exacerbated at the current time by material limitations that will be discussed briefly later.

First, any simple approaches using surface friction as a means for securing an elastomer in tension are thwarted by the nature of the system.  Friction forces depend both on high coefficients of friction and high normal forces to be effective.  Since the elastomer is being held in a chamber of hydraulic fluid at high pressure, it must be assumed to be lubricated and thus have a low coefficient of friction.  Since the elastomer thins (quite significantly) along its length as it is stretched, the normal force that it can exert on friction clamps decreases precisely when the need for gripping forces are highest.

Second, the exceptionally high strains to which the elastomer is necessarily subjected render barbs and other surface impingements ineffective as the material easily

deforms around them.  Add to that the fact that adhesives do not bond well to elastomers, and the options for gripping become fewer and fewer.

Third, since conventional gripping methods have been developed for strains more than ten times smaller than those required for elastomers, they all ignore one of the primary problems present when gripping materials under high strain, contact continuity. When a grip either externally or internally engages a material surface, it does so along some subset of the surface.  This contact area is often made up of disjoint areas contacted by multiple gripping surfaces, but can in the case of rigid materials be a single continuous area contacted by a single continuous gripping surface.  This is one of the advantages of machine collets, they engulf almost the entire perimeter of a specimen, thus well distributing the gripping forces.  Split-hub clamps likewise engage almost the entire perimeter of shafts they are affixed to.  The problem with these and most rigid gripping methods is that while they can be manufactured to engage a particular perimeter continuously, they cannot adapt their gripping surfaces to engage a perimeter that shrinks. To do so would require gaps in the gripping surface which close as the specimen shrinks. While this method is well suited to gripping a variety of rigid specimens, it cannot accommodate elastomers.  Elastomers gripped by a disjoint set of surfaces will squeeze into the gaps between the surfaces as they are compressed.  While small gaps, with sufficiently smooth transitions may be acceptable for small strains, large gaps needed to create large strains inevitably result in pinched material as the elastomers fight to retain their initial size and shape.

The preferred method for gripping soft materials under high strain would be to fashion the material with a gage length much thinner than its gripped ends.  While these

large ends might increase the overall volume of the system undesirably, they could be secured by any number of simple means because the strain they undergo in the process of holding the thinner gage length in tension would be much lower than that which the gage length experiences. However, the problem with this method is also twofold. First, this requires material samples to be obtained with non-uniform cross-sections. Custom samples are not readily available from suppliers of high performance polyurethanes, and the mixing, casting, and curing of custom samples is precarious, with poor material uniformity even under the best of circumstances. Small internal bubble or surface defects become crippling stress concentrations under high strains. Second, this method requires grips and gripping sections of the elastomer to much larger profiles than that of the elastomer gage length. If everything is to fit within a pressurized hydraulic cylinder, the ratio of dead volume to volume of the elastomer gage length is undesirably large. After considering both of these problems, it was determined that a method for gripping uniform cross-sections of high strain elastomer should be prioritized.

### 2. Opposing conical clamps

The first design proposed was developed for the gripping of a hollow, thick-walled elastomeric tube. A doubly tapered brass bulb with a blind, tapped hole in one end was threaded onto a steel tube which would serve as the cap-side anchor or a similar peg connected to a hydraulic piston. The tube and bulb would be rammed into one side of the elastomer. Afterwards, a brass collar with a slight conical interior taper would be forced onto the end of the elastomer. As the elastomer becomes stretched, the sheer motion

between the two matching tapers forces the two together, further compressing the elastomer within the closing gap between them. In this manner, the friction forces between the involved surfaces increases rather than decreases as the elastomer is stretched.

Figure 27 Progression of Bulb and Collar Design

Two key difficulties in this approach made it untenable within the scope of this project. First, the optimal taper slope, size, and shape seemed impossible to determine analytically as the tradeoff between maximum gripping force and required assembly force is dependent not only upon all of these variables, but also upon surface friction, and the time required to manufacture each set of brass tapers, combined with the unsolved problem of easily and repeatably quantifying their effectiveness, made experimental optimization unrealistic. Second, because elastomers are virtually incompressible, driving the brass collars onto the elastomer tube ends proved to be difficult even for softer polyurethane, even without the steel tubes and brass inserts in place. The harder one tries to drive a sample of polyurethane through a brass collar, the more the sample tries to expand against the collar walls. The greater the driving force, the greater the

resistive force, both in terms of normal force and consequent friction. Since the prime material candidate has a stiffness around ten times that of the softer polyurethane, the design was shelved in search for one that could be assembled without heavy machinery.

### 3. Continuous Perimeter Clamp

Since both 40A and 90A durometer polyurethanes are available in square cross-section bars of appropriate sizes and aspect ratios for small scale accumulators, focus was next turned to the development of a gripping technique for such bars. A device was designed whereby a ring of slidably engaging gripping components would slidably engage the polymer surface in a way that would maintain a continuous (with seems) perimeter of gripping area that could be enlarged or shrunk actively in a relatively low profile.
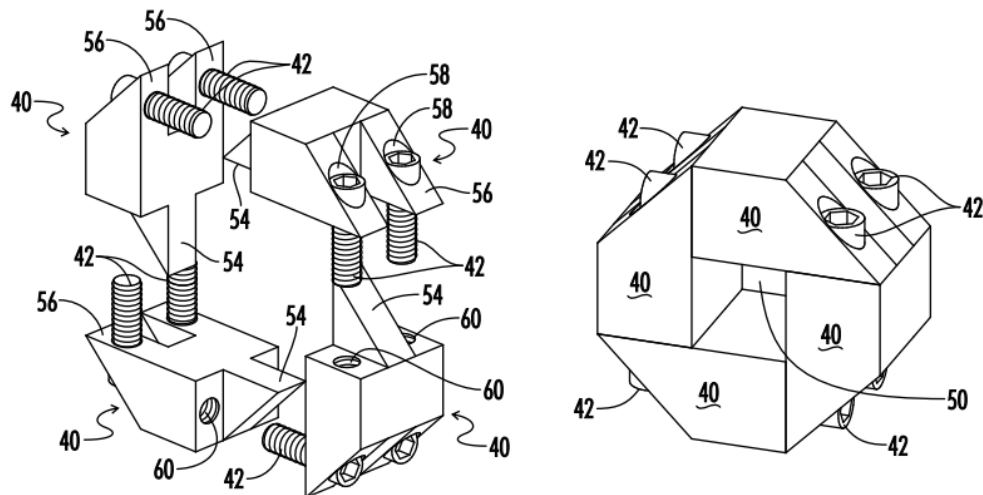


Figure 28 Continuous Perimeter Clamp Schematic from Patent App.

In the case of a square specimen, a Continuous Perimeter Clamp (CPC) has four identical components with each component having three layers. The central layer of each component slidably engages the central layer of its two adjacent components in order to form the continuous perimeter. These layers are driven closer together by the two outer driving layers, which in Figure 28 are depicted as identical but reverse-facing versions of the central layer. As the driving layers pull themselves towards each other, the mating surfaces of the driven layers are pulled past one another. This motion keeps a constant gripping shape which decreases uniformly without gaps that would allow material to escape. The maximum range of travel of a CPC is dependent upon the aspect ratios of the central layer surfaces. The clamp depicted in Figure 28 can reduce its initial bore cross section by 75% (from 3/4" x 3/4" to 3/8" x 3/8"), resulting in a compressed material state equivalent to 300% uniaxial tensile strain. In practice, a thin layer of nylon was wrapped around specimens before insertion into the CPC both in order to protect the material surface from any metal edges and to further compress the final material as the nylon took up some of the 25% remaining area. Because the CPC is screw driven, it is relatively easy to assemble, requiring much less torque than any of the following wrap-based methods.

4. Internal bulb-external wrap

Although the continuous perimeter clamp performed well for square bar specimens, both the shape of the specimens and the size of the clamps proved to be too limiting on the ratio of fluid volume to elastomer volume. Since this volume ratio is

essential to the curve flattening performance of the distributed piston accumulator, a new grip was needed with both a very low profile and elastomer tube compatibility.

A revisit of the problems that the conical clamps had when gripping 1" x 3/8" polyurethane tubes provided some insight into new methods for this next generation of grips. Longer, shallower brass bulbs were machined that would be easier to ram into the tube ends. Instead of machining brass collars to form the external taper, nylon rope was tightly wrapped along the length of the insertion. This shell of rope was able to squeeze the tube wall without damaging it and would be virtually inextensible once wrapped, forming a tapered collar to match the bulb inserts. Figure 29 depicts the first prototype using this method, with the aforementioned polyurethane tube anchored inside of a 1" bore polycarbonate tube.



Figure 29 Internal Bulb-External Wrap in Use in Tube Prototype

Securing the rope ends proved difficult, as the nylon was not able to squeeze the tubes enough to allow room for a knot to be tied. A coating of epoxy on the bands provided a temporary solution which allowed for testing of a tube of 40A polyurethane. Unfortunately, this setup could not be used to grip 90A polyurethane in its current state for various reasons. The brass inserts could not easily be rammed into the stiffer tubes

66

despite their gentle taper. The internal threads of the bulbs were not projected to be strong enough to hold the much higher tensile loads that 90A would demand. The nylon rope was not strong enough to sufficiently compress the 90A, and the epoxy coating, barely strong enough for the low pressure prototype would be entirely insufficient at higher pressures.

### 5. Internal channels-external wrap

In order to address the problems of the internal bulb-external wrap setup, new anchors were machined from steel with maximum diameters no greater than the inside tube diameters. Instead of bulging outward to form a taper, tapered channels were lathed into the anchors. It was reasoned that if the polyurethane could be wrapped tightly enough from the outside it would be unable to work its way in and out of the channels during loading. To achieve these wraps, Kevlar thread was procured which could put more pressure on the polyurethane. Later, when the breaking strength of the largest diameter Kevlar thread proved insufficient, Dacron braided polyester cord was introduced as a replacement with great success. Platforms were constructed to aid in the winding of the Dacron with cord tension well in excess of 100 lbs. Unfortunately this too ultimately proved insufficient as two variations of steel inserts continued to slip out of the tubes, pushing back the polyurethane walls as they went. With a maximum achieved cylinder pressure of less than 300 psi—compared to the target pressure of 800-1200 psi— efforts were turned from modification to complete redesign.

## 6. Tiered plug-external wrap

The chief problem with the above method is that wrapping tightness and distribution among the channels was difficult to quantify and varied greatly from trial to trial. It was observed that in each case of anchor slipping, the external wraps remained fixed at their place along the polyurethane tube. The polyurethane did not work its way around the wraps, but rather the anchor worked its way through the polyurethane folds by crushing them outwards against the Dacron collar. So long as the anchors themselves had room to pass through the wraps, friction and material stiffness, both difficult to quantify in this case, were all that held the anchors in place. If the Dacron could somehow be tightened to an inner diameter less than the thickest anchor region, it would be impossible for the anchor to slip through. In order to achieve such tightness with the tools available, it was necessary to greatly reduce the diameter of the anchor section around which the wraps were tightened. Unfortunately, the expected tensile forces prohibited such reductions as the anchor stresses would surpass the yield strength of readily machineable steel. To circumvent this problem, an three-piece anchor was designed. One piece contained a 0.375" diameter bulb that would slide snugly into the polyurethane tube and which tapered down to a short section of 0.250" rod onto which the wrapped portion of the elastomer would eventually settle. The end of this rod was threaded to anchor to either the cylinder end or the hydraulic piston with ¼" - 28 threads large enough to hold the full test loads. After these threads the rod tapered further to thread into another 0.250" section of steel. This second piece was tapered on its far side to provide a smooth transition to a 6-32 bolt onto which it was threaded. The assembled

product was a slender rod which transitioned down from 0.375" to 0.138" in two stages. A combination of epoxy and Teflon tape ensured a smooth, continuous surface along its length. Once it was inserted into a polyurethane tube, Dacron could be wrapped to the proper tightness along the section containing the 0.138" bolt.



Figure 30 Evolution of External Wrap Grip Technique

The bolt ends of two opposing anchors could then be gripped in a tensile load cell and pulled until the 0.250" section of the anchors wedged their way into position within the Dacron collar. The bolt and adapter stages of each anchor could then be removed, and the exposed ¼" - 28 threads could be screwed into their respective anchoring points. So long as the Dacron collar was tightened to an inner diameter between 0.375" and 0.250", the anchors would now be incapable of slipping.
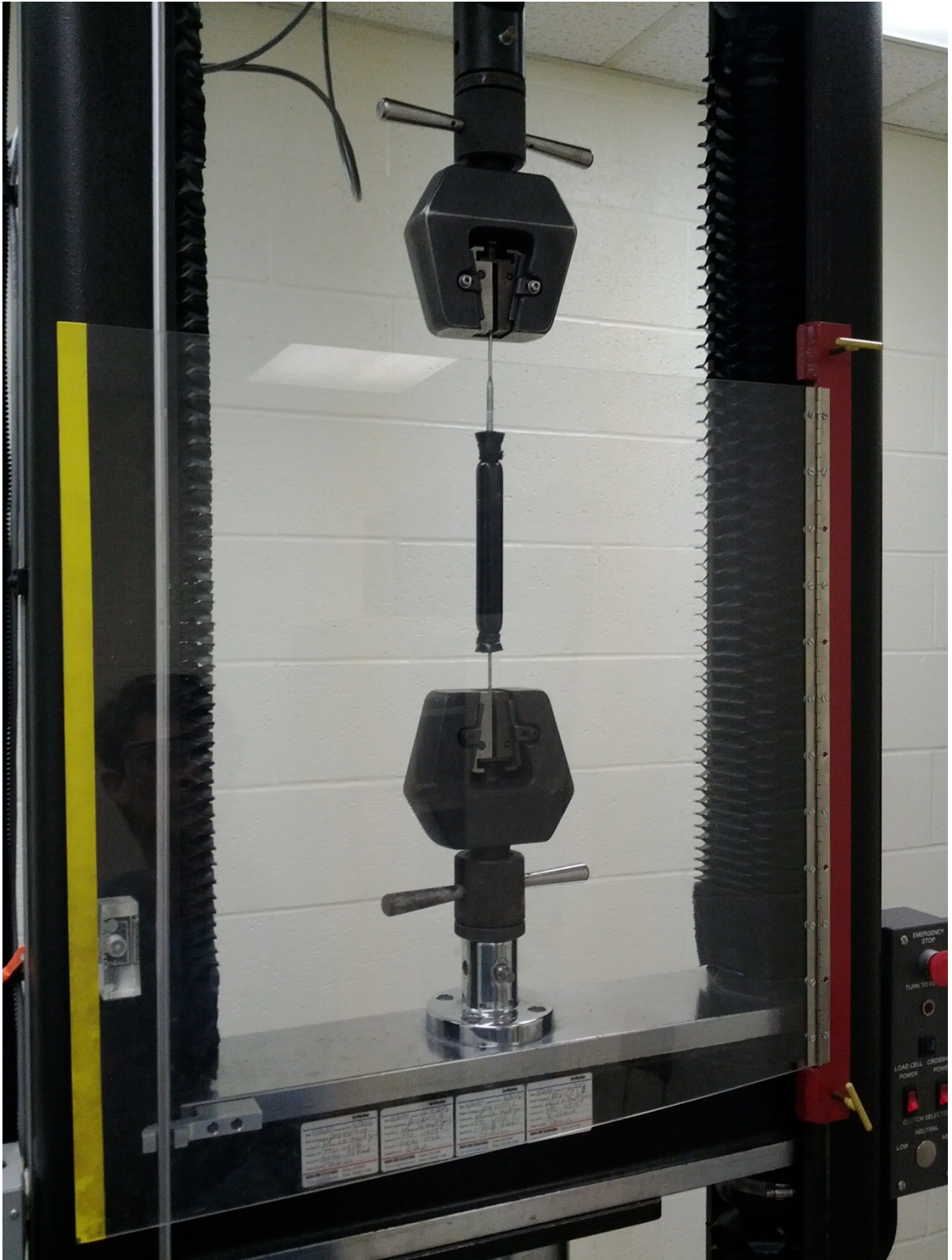
Figure 31 Tiered-Plug being Pulled into Position

CHAPTER 7

**Distributed Piston Low Pressure Prototypes**

1. Square-bar Setup (up to 55 psi)

In order to move towards a more realistic representation of an actual accumulator, driving fluid for all remaining prototypes was changed from nitrogen gas to hydraulic oil 32. A Baldor VM3537 electric motor was used to drive Oildyne miniature piston pumps which pumped fluid from a reservoir through a check valve and into the accumulator. A bypass valve allowed fluid to flow around the check valve back into the reservoir during discharging. Pressure data was again acquired via a Kulite XTL-190-5000A pressure transducer with analog filtering and amplification. Position of the devices was tracked by attaching an optical encoder to the end of the piston rod which would measure position incrementally as it moved along a linear encoder strip. Closed loop position control drove the motor via a Baldor VS1ST Microdrive servo amplifier.
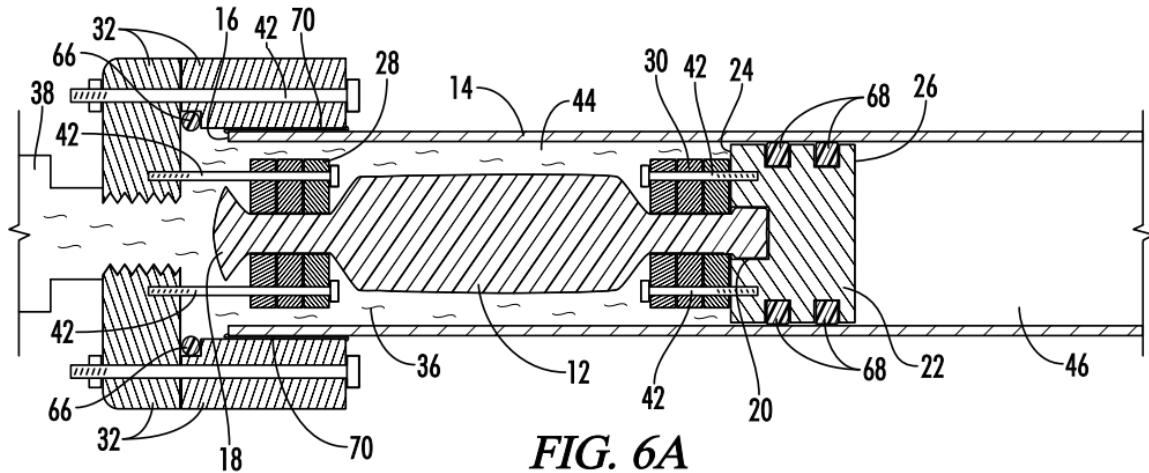
Figure 32 Square Bar Prototype Schematic from Patent App.



Figure 33 Square Bar Prototype Actual

The first distributed piston accumulator prototype utilized continuous perimeter clamps to grip a 0.75" x 0.75" x 6" 40A polyurethane bar, squeezing it down to less than 25% of its initial area at the grips. These clamps had an outer diameter of just under 1.25", allowing them to fit smoothly into a polycarbonate tube that would be used as the hydraulic cylinder. A piston was fashioned out of aluminum and polyurethane cup seals which provided a low-friction sliding seal at pressures up to 300 psi.

The selection of aspect ratio and the bulk of the continuous perimeter clamps both prevented much information from being gleamed from this setup. The relatively long gage length of the specimen prevented strains in excess of 125% from being reached, and the high initial ratio of fluid volume to elastomer volume minimized the curve-flattening properties of the distributed piston design. Still, this prototype served as a test bed for the hydraulics and electronics that would be used for all the prototypes that followed. In addition, it demonstrated that high round trip efficiencies (averaging in excess of 88% for this setup) could be achieved in an elastomeric accumulator.
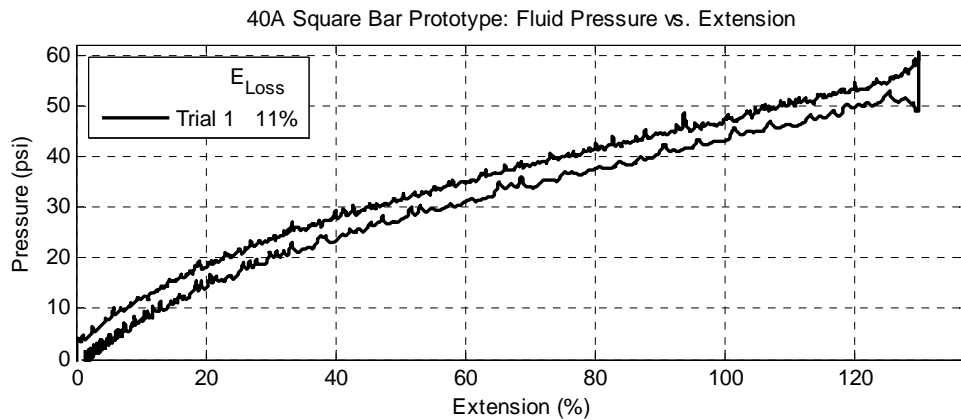
Figure 34 Square Bar Prototype Round Trip Efficiency

## 2. Tube Setup (over 150 psi)

The next logical step in prototype development was to decrease the clamping profile and the initial ratio of fluid volume to elastomer volume. The internal bulb-external wrap grip was used to secure a 1"OD x 0.375"ID x 12" tube of 40A polyurethane within a 1" polycarbonate tube. Once again the limited stroke of the setup prevented high strains from being reached, with the maximum strain being 150%.

However, this setup provided a highly reduced volume ratio from 1.18 to 0.16. With this ratio the curve flattening effects of the distributed piston can be easily seen, even though the stroke was limited.

In order to simplify the construction of the device, the inlet port was modified to serve as the anchor point for the cap-side anchor. A compression tube was passed through the port into the chamber and given external threads onto which a brass bulb was mounted. Holes were drilled in the tube sides to allow fluid to flow into the chamber.



Figure 35 Hollow Tube Prototype

This design, while compact, provides very narrow passageways for fluid flow and likely contributed heavily to the inefficiency of this device. Having the inlet port located behind the end of the elastomer also chokes fluid flow as it must flow around this unstretched section in order to reach the rest of the chamber. Because 40A polyurethane is much softer than 90A it is also difficult to selectively remove material. As such, the very ends of the elastomer, being removed from the tensile loading, remained unstretched throughout the trials and tended to drag along the cylinder walls, further reducing efficiency.

As stated above, the large inefficiencies introduced by various aspects of the setup removed round trip efficiency as a potential subject for observation in this prototype. Like the previous prototype, this one also had severe limitations in regards to maximum

pressure and displacement. However, it did demonstrate well the desired curve effects that were predicted for distributed piston accumulators of low fluid/elastomer volume ratios.

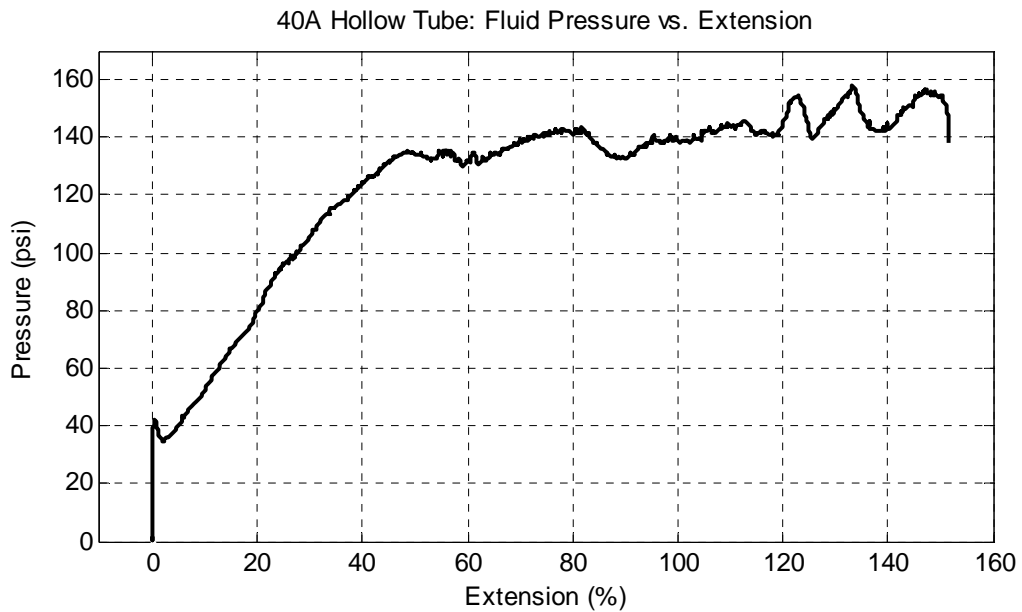**40A Hollow Tube: Fluid Pressure vs. Extension**



Figure 36 Hollow Tube Filtered Charging Pressure

As seen in Figure 36 the low initial fluid to volume ratio did produce the expected curve flattening results. It now remained to be seen if this effect could be utilized on polyurethane 90A at much higher charging pressures.

CHAPTER 8


**High Pressure Prototype**


1. <u>Changes from low-pressure setup</u>

Now that both the distributed piston effect and round trip efficiencies had been demonstrated, the next step was to build a high pressure prototype that would apply these principles to a realistic volume of the candidate material. If successful, the move from single prototype to full scale accumulator would simply be a matter of arranging multiple devices in series and parallel configurations. A 1" bore hydraulic cylinder rated up to 1500 psi was procured from industry partner Bosch Rexroth, and the piston and cylinder were modified to provide anchoring sites for multiple grip designs. As stated above in the section on gripping, the anchoring of 90A polyurethane at high strains in a small package proved to be an ongoing problem. Multiple iterations of the internal channels-external wrap method led to anchor slip at pressures ranging from 200 to 400 psi. However, eventually the tiered plug-external wrap technique emerged as a viable solution.



Figure 37 High Pressure Hydraulic Cylinder

While that work was ongoing, a new problem emerged in the form of an unforeseen pressure ceiling. The hydraulic pump-motor setup appeared to be incapable of generating pressures much higher than 400 psi. While it is rated for more than 1500 psi, these ratings assume a higher steady state flow rate than is appropriate or even possible for a single accumulator device. As pressure approached 400 psi, the slow moving motor would stall out, even with a saturated command signal to the servo amplifier. The exact pressure values needed to stretch a sample of polyurethane are impractical to predict analytically, given the complex shape and loading of a distributed piston device and the nonlinear behavior of hyperelastic materials. However, rough projections indicated that pressures in excess of 1200 psi would likely be required to achieve 300% strain. Since this seemed untenable with the current pump-motor limitations, it was decided that a moderate pressure test would be performed by stretching another sample of 40A polyurethane, this time to 300% strain.

## 2. Safety measures

In anticipation of potential fitting leaks, each hydraulic fitting that would contain high pressure fluid was encased in a capped, clear PVC pipe section that would both contain and draw attention to leaks should they occur. The inlet to the high pressure end of the cylinder was similarly encased with a polycarbonate shield.

## 3. Results and conclusions

The highest pressure trial recorded with this distributed piston setup before slip was 350 psi. This corresponded to a material strain in the 90A polyurethane sample of about 25%.

**90A DPEA: Fluid Pressure vs. Extension**
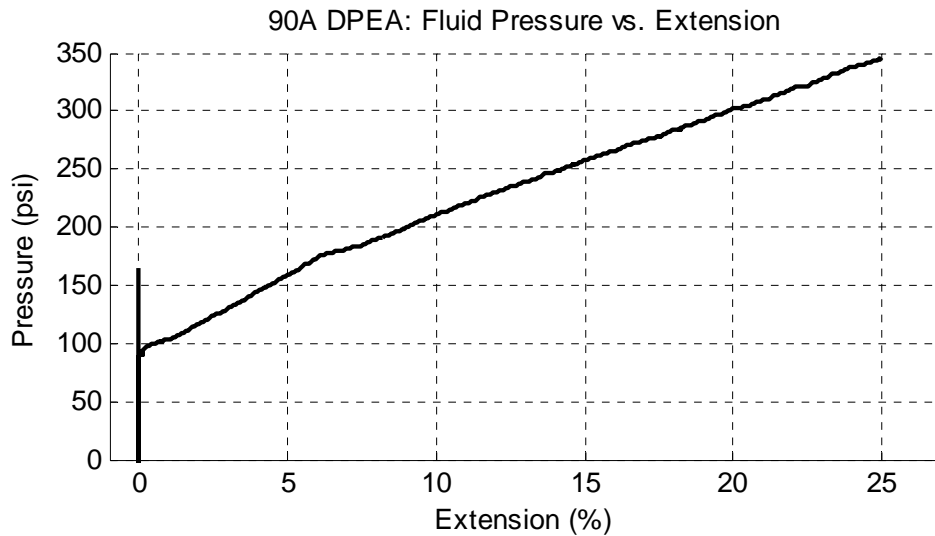
Figure 38 DPEA Accumulator Charging Pressure before Anchor Slip

Extrapolation of this value to higher pressures would be impractical considering the complexity of the distributed piston effect combined with the hyperelasticity of the material. However the 40A polyurethane trials, while at lower pressure, give more information. A direct comparison between a sample stretched in the distributed piston cylinder and the same sample stretched in a tensile load cell show that the relationship between fluid pressure and material stress does indeed vary greatly throughout the piston stroke.

40A Tensile Stress and DPEA Pressure

Legend:
- Tensile Load Cell: $S_{avg} = S_{max} * 64\%$
- DPEA Pressure: $P_{avg} = P_{max} * 71\%$

Y-axis: Stress, Pressure (psi)
X-axis: Strain (%)

Figure 39 Comparison of DPEA to Tensile Testing

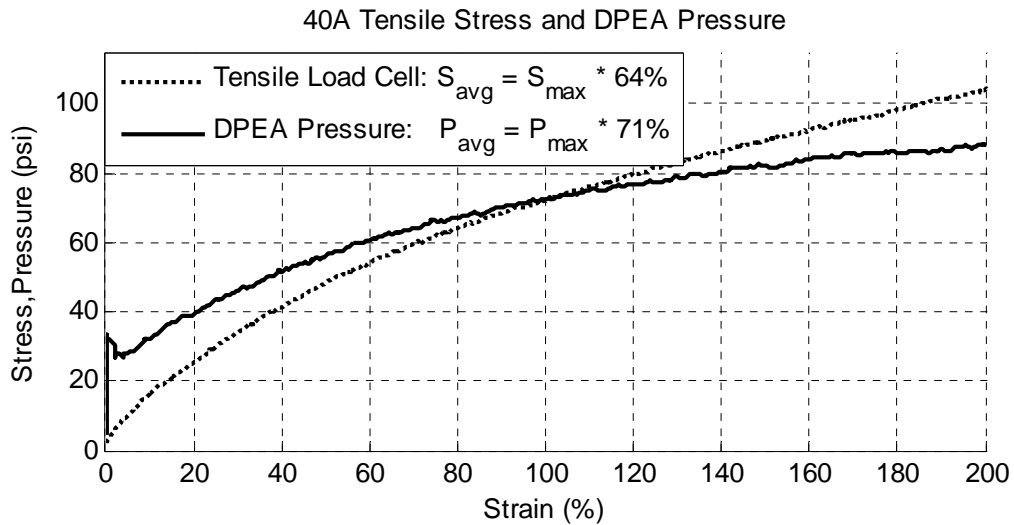At low strains the fluid pressure is significantly (more than 100%) higher than the material stress. At 100% strain the two values are virtually equal. By 200% strain, the material stress is actually 20% higher than the fluid pressure. This behavior, which is believed to be dependent upon the geometry of the elastomer rather than its material properties, has been measured as a range of ratios between fluid pressure and material stress over a range in material strain. Figure 40 shows the result of applied these ratios to tensile test data for polyurethane 90A (from Figure 14) in order to obtain a prediction of approximate pressure values for a DPEA containing a 90A specimen of these same aspect ratios.

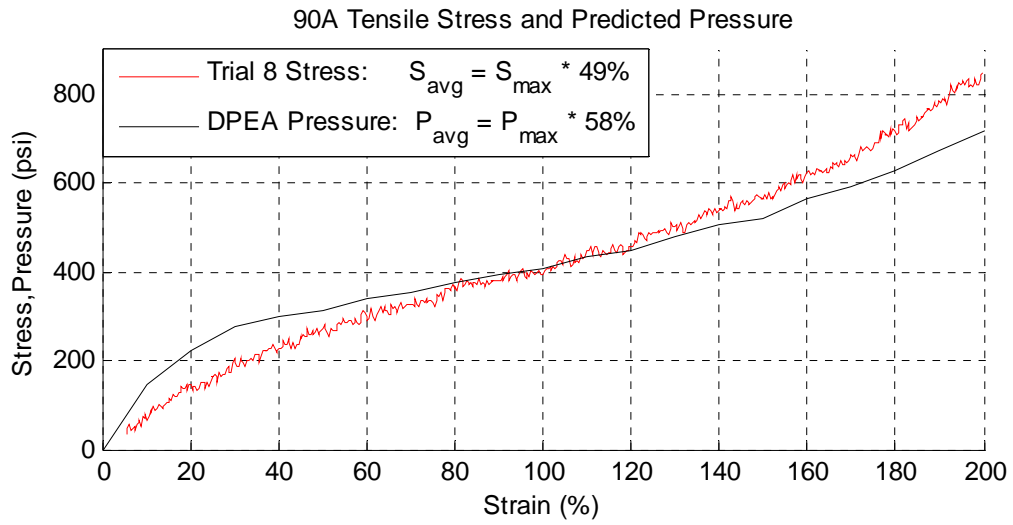**90A Tensile Stress and Predicted Pressure**

Figure 40 DPEA Effect Applied to 90A Tensile Data

The benefits of curve flattening can be readily seen here as the ratio of average-to-maximum effort increases from 49% in the case of tensile stress to 58% in the case of DPEA pressure. Recall that having a higher average-to-maximum ratio translates directly into having a higher hydraulic energy density.

CHAPTER 9


**Conclusions and Future Work**


In this thesis, several designs of strain-energy accumulators have been described, and many of their benefits and drawbacks, both theoretical and observed, have been put forward in order to demonstrate some of the multitude of considerations that must be taken into account in the implementation of a strain-energy accumulator. From the simple bladder one can learn of the importance of material utilization and the dangers of dead volume. From the diaphragms in series we learned that the very nature of a design can place stringent restrictions on maximum material strain, independent of scaling. Though the house-grille bladder, rack and roller, and hinged harp were never prototyped, they provide strong examples of the ways in which variable mechanical advantage might play a role in shaping accumulator force and pressure profiles. The distributed piston accumulator prototypes validated the theory of P-V curve shaping and served as platforms for demonstrating potential round-trip efficiencies and gripping techniques. They also brought to light the problem of envelope volume and how large the path from material energy density to system energy density can be.

It is the recommendation of this author that the first steps in future work should be a twofold exploration of the limits of uniaxial compression. The motivation behind this recommendation can be found in the supplemental chapter 10. First, the optimal material and stress limits for maximizing material energy density in compression must be determined. This search should begin with but not be restricted to thermoset

polyurethanes of similar hardness to the 90A polyurethane explored in this thesis. Second, the limitations on round trip efficiency for a squat specimen compressed between two plates must be pursued. This could be done via the use of a hydraulic cylinder containing a low friction anvil and piston between which an elastomeric cylinder can rest. The compression chamber must be well lubricated but also be open to atmosphere to prevent the volume change of the chamber from putting backpressure on the piston.

Another area which must be explored if elastomeric accumulators are to make their way into the hybrid vehicle industry is the effect of temperature, both ambient and generated, on accumulator performance. While some thermoset elastomers are engineered to withstand high temperatures, a thorough study of efficiency and energy density over a range of operating temperatures is required.

Because of limitations in precision, the effects of strain rate were not possible to quantify with the setups used. High frequency strain testing on the order of 0.3 Hz should be performed in order to ascertain any effects that rapid braking would have on the elastomer efficiency and fatigue life. High frequency tests would also permit the observation of the thermodynamics of the elastomers. When elastomers are stretched, some of the work done on the material is reversibly converted to heat, raising the temperature of the material somewhat. When released, this energy is returned, and the material cools. If this temperature change is significant enough, some of the energy may be lost to the environment. The reverse however is also true, a deformed elastomer become stiffer (and therefore capable of doing more work) when heated. Therefore, if the effect is significant enough and well understood, it may be exploitable. A strong heat source, like the engine of a car, could be used to overcharge the elastomer to an elevated

temperature once it has been stretched. This energy would be converted into additional work by the elastomer during the discharge phase. (Lyon 1984)

Lastly, once the design of an accumulator, combined with improvements in elastomer properties, has reached a point where system energy density and efficiency have reached levels appropriate for hydraulic regenerative braking in smaller vehicles, the last hurdle to full scale implementation is the control and transmission of power to and from the accumulator. While these schemes will likely be based upon those which govern current gas accumulator designs—like those employed in refuse trucks by Eaton Corp.—they will almost certainly need to be tailored to incorporate the effort profile of the elastomeric accumulators, as this profile will necessarily be a significant departure from and improvement on that of gas accumulators.

### Contributions

- Demonstrated cyclical energy densities of polyurethane in tension and compression

- Demonstrated an application of fluid mechanical advantage for use in effort-flow profile shaping

- A simple and effective solution for high gravimetric energy density accumulator. (Hinged Harp)

- A high strength, easy to assemble clamp design for gripping high strain, constant-cross-section, solid core elastomers (Continuous Perimeter Clamp)

- A high strength, low profile method for gripping high strain, constant-cross-section, thick-walled, elastomeric tubes (Tiered-plug external wrap)

- Characterized primary and secondary design considerations for strain-energy accumulators

- Developed a generalized relationship between material energy density and overall system energy density as a function of maximum strain and demonstrated how pre-compression can impact this relationship

CHAPTER 10


**Supplemental on Uniaxial Compression**


In comparison to all of the aforementioned designs, uniaxial compression is a relatively simple concept that we were nonetheless reluctant to explore at first. Compression set—the amount of strain which remains in a material after compressive loading has been removed—can be quite high for some elastomers and can be very temperature dependent. Additionally, the surface friction generated when an elastomer is crushed between two rigid plates is proportional to the normal force acting on the material. These two elements led to the foregone conclusion that uniaxial compression would never match the round-trip efficiency of uniaxial tension. Since the contribution of friction in this matter is surface and lubrication dependent and therefore impractical to isolate, very little testing was done initially on specimens in compression.

However, as testing of various piston prototypes was being concluded, the decision was made to revisit uniaxial compression to assess the limits in energy density. It was believed that a specimen under compressive loading would have less energy storage capabilities than one under tensile loading since it travels through a smaller space in the direction of driving force. Indeed, the first rounds of testing showed that a specimen crushed to 25% of its initial height stored less than 10% of the energy per unit volume required to stretch a specimen to four times its initial length. The quandary here is how to equate the two forms of strain. Engineering strain, simple to define and understand for a sample in uniaxial tension, makes less sense in the case of uniaxial

compression. Strain values in one do not easily map into strain values in the other, neither in terms of energy required nor—as would be seen in later tests—in terms of material strength. A material which fails in tension at a strain of 500% for example, does not fail when it is compressed to 1/6th of its original height, as was observed in later testing.

In an effort to get some idea of the efficiencies possible in the case of a lubricated specimen, a bar of 90A polyurethane was placed in the high pressure hydraulic cylinder setup on one side of the piston, while high pressure fluid was used to ram it by pumping fluid into the rod side. Unfortunately, the material was much too strong for our pump-motor operating in a reduced capacity, especially since the piston rod reduced the effective surface area on which the fluid could act. In an effort order to boost the pump-motor performance, the bypass valve was throttled in order to keep motor speed higher as it approached higher pressures. These efforts were met with some success and as a result pressures of 630 psi were achieved in one trial. A roundtrip efficiency of 78% was recorded (Figure 41), giving sufficient reason to pursue further energy density tests with a compressive load cell.
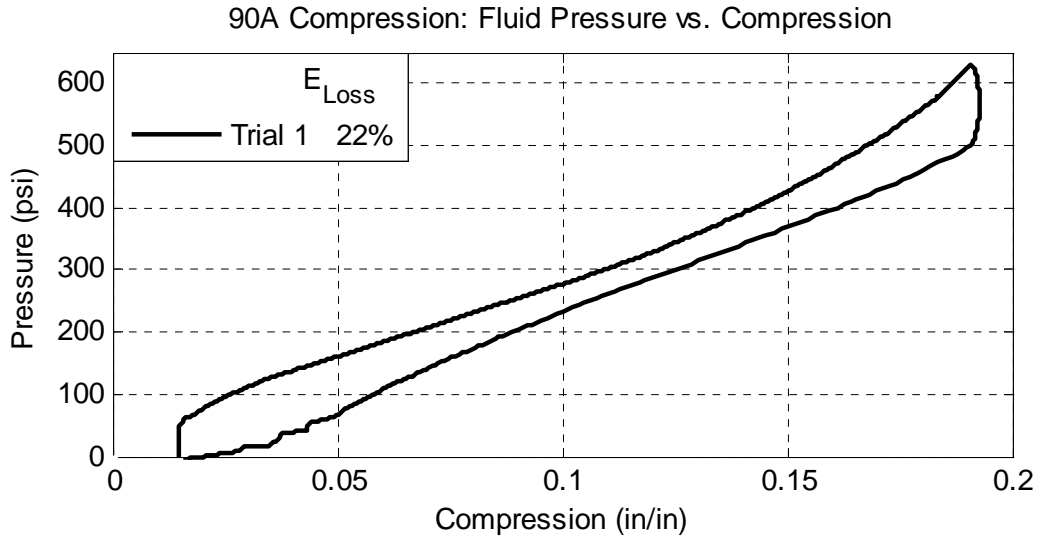
Figure 41 First Efficiency Tests for Lubricated Compression

This efficiency, though only demonstrated over a small strain range, was motive enough to perform load cell testing at higher compressive strains. Uniaxial compression requires much shorter travel distances than uniaxial tension, and so there was no reason to look for alternative, quick and dirty test rigs as was done with initial tensile testing, since the automated load cell would be able to acquire the necessary data very quickly. For this next phase of testing, small discs of polyurethane 90A were compressed using a load cell rated to 1100 lbs at a compression rate of 0.10 inches per minute. Because this load cell capacity is only 1/10th that of the tensile load cell, samples in compression were necessarily very small in diameter (less than 1/8 of an inch). In order to prevent buckling, this required sample heights to be similarly small. Even at these small diameters, the imposed load limit of 1000 lbs was reached before material failure in all cases. In fact, the limit was reached before any noticeable material degradation was observed. As the material was compressed, the stiffness increased rapidly, compounded by its increase in diameter. To avoid confusion regarding the meaning of engineering

87

stress and strain of materials under compression, the integral under the force-displacement curve of the load cell was used for calculating energy density. Unlike the specimens in tension, energy density appeared to increase at an increasing rate the further the material was compressed. Initial energy density and efficiency calculations calculated from the force-displacement curves were made. However, at this point it was discovered that an unforeseen complication was artificially raising the apparent deflection and thus energy density of compression trials. Because the size scale of compression is so small and the forces are so large, the steel beam upon which the polyurethane samples were resting was deflecting enough to store a significant amount of energy in its own strain. After the beam was replaced with a more rigid one, tests were done on the setup alone. Applying the 1000 lb force limit of the load cell directly on the steel beam revealed the reduced but still significant contribution of this deflection. Updated tests were done on the polyurethane sample at maximum load. Since compressive loads act like springs in series, the total energy stored in the setup and the polyurethane at a given load is equivalent to the sum that each stores alone at the same load. Therefore, the energy stored in the steel alone can be subtracted out directly from the total energy storage, revealing the true energy density of the polyurethane at the given loads. At 1000 lbs, the polyurethane demonstrated an energy density of 23 kJ/L and was compressed to 16% of its initial height.

Obtaining the full range of force and displacement for the polyurethane alone is a more complex problem. To achieve an estimate for the contribution of the steel deflection as a function of load, a polynomial fit x(L) was applied to the rising half of trial S5 (see Figure 42). The combined displacement data of trial 8 was scaled by (1-

x(L)) in order to yield T8-S5, the approximate force-displacement curve of the polyurethane. The integral under this curve, divided by $\forall_M$, is 23.4 kJ/L which closely agrees 23.6 kJ/L, the difference in the average energy densities of the combined trials and the steel-only trials.
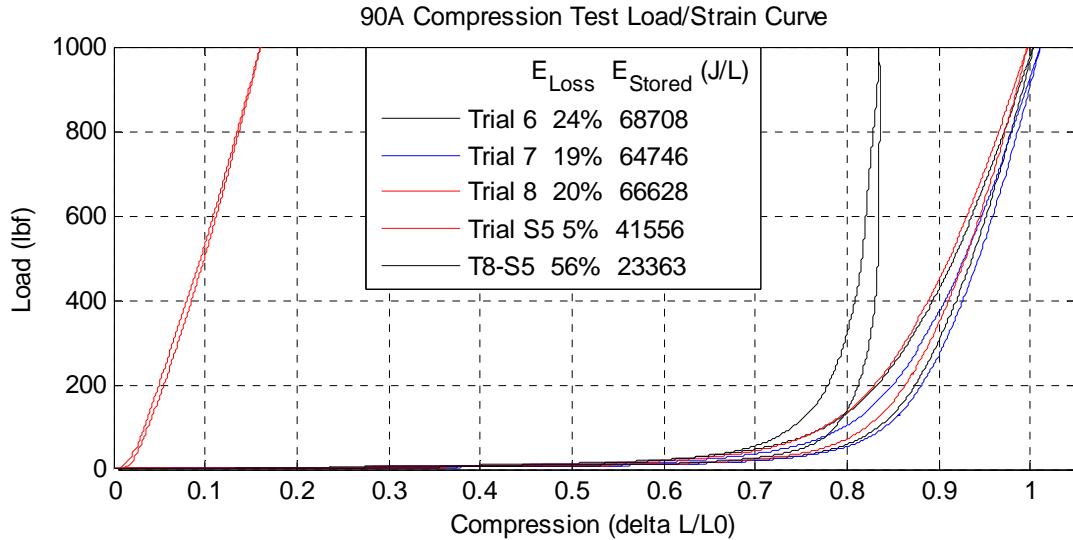


Figure 42 Uniaxial Compression Results, Combined and Separated

As seen from these tests, the energy density of polyurethane in uniaxial compression can be significantly higher than in uniaxial tension. The fundamental reason for this is still not understood, but one hypothesis centers around the idea of load distribution and failure mode. When a portion of a specimen in tension fails, it completely loses its ability to contribute to load bearing. The remaining cross-section of material now bears an increased load and stress rises. As a result, cracks within the material quickly propagate throughout, causing rapid and catastrophic failure of the specimen. When a short disc is loaded in compression, however, the failure mode is less obvious. Since buckling cannot occur at squat aspect ratios, the only remaining failure

mode is shear slip along diagonal shear planes. Most of the shear planes of largest stress, located at 45 degrees, terminate within the loaded ends of the material rather than the unsupported material walls. Because of this, displaced elements in compression still contribute to the overall material strength, and no mode exists for unstable compressive failure at certain aspect ratios. It is also possible that the strength of polyurethane in compression is due to the nature of crack propagation. In his analysis of the fatigue life of hard polyurethane in wheelchair tires, Kauzlarich cites Williams (Williams 1980) book *Stress Analysis of Polymers*, which contains an analysis for crack growth, saying "Crack growth is not promoted by compressive stresses; in fact it appears that compressive stresses inhibit crack growth. (Kauzlarich)"

Neither the ultimate nor the optimal compressive strengths of polyurethane 90A have thus far been determined, but the energy density has been demonstrated to be at least 50% higher than the same material in tension. Add to this the removal of the need for grips and gripped material, and the argument becomes quite strong for the pursuit of accumulator designs that capitalize on uniaxial compression. It remains to be seen if the problem of surface friction can yet be overcome at high loads.

Beyond the demonstrated gains in material energy density, uniaxial compression has one significant advantage to uniaxial extension. Recall equation (17) and its formulation. This equation gives a function for determining the minimum theoretical system volume of a specimen in uniaxial tension. The same approach can be used for calculating the minimum envelope volume of a specimen in uniaxial compression. Equation (17) lists $\frac{\forall_{Envelope}}{\forall_M}$ as a function of $\frac{l}{l_0}$ where $l_0 < l$, but this is purely a geometric relation. It does not specify which length is the relaxed length and which length is the

strained length. For a specimen under compression, this means that the volume ratio can

be written similarly as

$$\forall_{Envelope} = \forall_M \left(1 + ln\left(\frac{L_0}{L}\right)\right) \qquad (18)$$

Where $L_0 > L$. The advantage in compression comes from the fact that most of the

energy stored in a compressed material is stored in the tail end of compression. As seen

in Figure 43, for the sample of 90A polyurethane compressed in this experiment, the

material energy density displayed by the last 20% of travel alone was 18.6 kJ/L, more

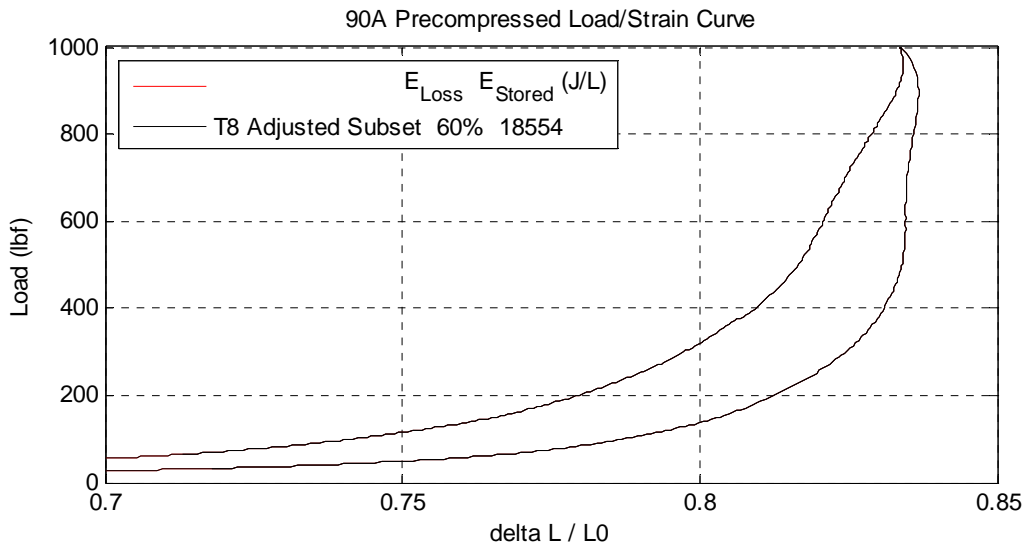than 79% of the maximum displayed energy density.



Figure 43 Subset of Last 20% of Compression Travel

This 80% reduction in travel means an 80% reduction in $L_0$. This decreases

$\frac{\forall_{Envelope}}{\forall_M}$ from 2.81 in the case of no pre-compression to 1.61 in the pre-compressed case,

a 43% reduction.  Recall again that the overall system energy density $e_{System}$ is limited by the inverse of $\forall_{Envelope}$. For the case of uniaxial extension, this value equates to be:

$$e_{System} \leq \frac{1}{\forall_{Envelope}} = \frac{15.4\text{kJ/L}}{2.39} = 6.44\text{kJ/L} \tag{19}$$

For the case of uniaxial compression, this value comes out to be 8.28 kJ/L with no pre-compression. For a sample pre-compressed to 30% of its original length, this value jumps to 11.5 kJ/L, a 39% increase from the compression baseline and a 79% improvement over the best-case of uniaxial tension.  The optimal ratio of pre-compression will undoubtedly vary for different polyurethanes, but its potential contribution to overall system energy density is substantial.

References

a. Tobul Accumulator, Inc.
   www.tobul.com/index.php?option=com_content&task=view&id=13&Itemid=27
b. Toulson, E. R. Evaluation of a Hybrid Hydraulic Launch Assist System for use in Small Road Vehicles, IEEE 4677190 (2008)
c. Diani, J, B. Fayole, P. Gilormini, "A review on the Mullins effect" European Polymer Journal. Volume 45. Issue 3. March 2009 (pages 601-612)
d. Gerlach, D.W. "ANALYSIS OF ELASTOMER REFRIGERATION CYCLES" International Refrigeration and Air Conditioning Conference. Paper 538 (2002)
e. Lyon, R.E. "Polyurethane-Urea Elastomers as Working Substances in Rubber Heat Engines" Journal of Applied Polymer Science Volume 29 Issue 9, (1984)
f. Pedchenko, A. V. "Design and Finite Element Modeling of a High Energy Density Strain Energy Accumulator" 2011
g. Pleiger Plastics Company www.pleiger.com/comp2.html
h. Kauzlarich, J. J. "Wheelchair tire rolling resistance and fatigue" Journal of Rehabilitation Research and Development Vol. 22 No. 3. BPR 10-42 Pages 25-41
i. WILLIAMS, J.G. *Stress Analysis of Polymers* (2nd ed .).Halstead, 1980. (Ellis Horwood Series in Engineering Science)
j. Karnopp, D. C, D. L. Margolis, R.C. Rosenberg. *System Dynamics: Modeling and Simulation of Mechatronic Systems*. Third Edition (Pages 18, 46-52) (2000)
k. Tucker, J. M, E. J. Barth, U.S. Patent Application No. 60105118, Unpublished (filing date Dec. 16, 2011)